Palaeogeography, Palaeoclimatology, Palaeoecology 699 (2026) 113992

Contents lists available at ScienceDirect

Palaeogeography, Palaeoclimatology, Palaeoecology

journal homepage: www.elsevier.com/locate/palaeo

A 10,000-year record of environmental change and human forcing in the Po Delta (northern Italy)

S. Catena [a], V. Rossi [a,*], M. Cacciari [b], A. Vecchi [a], M. Marchesini [b], S. Marvelli [b], S. Giuliani [c], L. Bellucci [c], C. Pellegrini [c,1], A. Amorosi [a,1]

[a] Department of Biological, Geological and Environmental Sciences, University of Bologna, Via Zamboni 67, 40126 Bologna, Italy
[b] Laboratorio di Palinologia, C.A.A. "Giorgio Nicoli", Via Sant'Agata 835, 40014 Crevalcore, (BO), Italy
[c] Istituto di Scienze Marine (ISMAR-CNR), Via Gobetti 101, 40129 Bologna, Italy

ARTICLE INFO

Editor: Laura Sadori

Keywords:
Palynology
Facies analysis
Climate change
Late Holocene
Little Ice Age

ABSTRACT

Deltaic successions are complex archives of both natural and human-driven landscape changes, which govern the preservation and temporal resolution of palaeoenvironmental signals in the stratigraphic record. Integrated sedimentological, meiofaunal, and palynological analyses of a 40 m-long borehole, constrained by a robust chronological framework based on radiocarbon (^{14}C) and short-lived radionuclide (^{137}Cs, ^{210}Pb) dating, delineate Holocene vegetation changes and environmental evolution in the Po Delta area. High-resolution stratigraphic analysis, supported by the identification of six pollen zones and ten subzones, highlights the strong potential of stratigraphically expanded, prograding deltaic successions to preserve records of environmental change particularly over the last ~2500 yr B.P. These records reflect the combined influence of climatic variability, anthropogenic activity, and catchment dynamics, providing an integrated view of landscape evolution across the land-sea continuum. Transgressive, open-bay to inner-shelf deposits document the rapid landward shift of the shoreline during the Early-Middle Holocene. This interval, associated with depositional hiatuses and stratigraphic condensation (0.11 cm/yr), records early afforestation, punctuated by short-lived phases of climatic deterioration, followed by the establishment of persistently warm and humid conditions during the Holocene Climatic Optimum. The 31-m-thick Late Holocene succession of prodelta, delta-front and delta-plain deposits, accumulated under increasing Po River influence and high sedimentation rates (up to 8 cm/yr), provides centennial- to sub-centennial-scale resolution of vegetation-based environmental and climate variability. Pollen assemblages record the onset and progressive intensification of human impact since the Iron Age. Despite strong anthropogenic forcing over the last two millennia, climatic signals remain clearly detectable in the pollen record, which captures short-lived episodes of regional cooling, including the onsets of the Late Antique Little Ice Age (LALIA) and Little Ice Age (LIA), as well as associated intervals of reduced solar activity.

1. Introduction

The Holocene represents a key period for unravelling high-frequency post-glacial climatic and environmental dynamics (Walker et al., 2012). Despite being milder than most of the Pleistocene, it was characterized by numerous short-term variations in temperature and/or humidity (e.g., Bond et al., 1997; Mayewski et al., 2004; Wanner et al., 2011), accompanied by changes in sea level (Lambeck et al., 2011), fluvial activity (Stanley and Warne, 1994; Besset et al., 2019), and vegetation (Allen, 2003; Kaplan et al., 2009; Roberts et al., 2011). Human activity progressively intensified during the Holocene, becoming a major driver of environmental change (Renaud et al., 2013; Anthony et al., 2014), particularly in the Mediterranean, where cultural landscapes emerged at least from the mid-Holocene (Magny et al., 2007; Mercuri et al., 2012; Sadori et al., 2013; Mercuri and Sadori, 2014). Evidence of human impact is preserved in various geological archives (Ruddiman, 2003; Dusar et al., 2011; Berger et al., 2016; Gibling, 2018), especially sediment cores, enabling multi-proxy reconstructions of landscape evolution and its driving forces (Birks and Birks, 2006; Last and Smol, 2006; Pellegrini et al., 2021).

* Corresponding author.
E-mail address: veronica.rossi4@unibo.it (V. Rossi).
[1] These authors contributed equally as senior authors

https://doi.org/10.1016/j.palaeo.2026.113992
Received 29 March 2026; Received in revised form 10 June 2026; Accepted 18 June 2026
Available online 19 June 2026

Fossil pollen represents a valuable proxy for palaeoenvironmental studies and coastal areas are ideal settings for reconstructing Holocene landscape dynamics, as they record the interplay of natural processes (e.g., sea-level fluctuations, river discharge, subsidence) and human activities, including land use, agriculture, and hydraulic interventions (Di Rita et al., 2015, 2022; Ghilardi et al., 2023, 2026; Kaniewski et al., 2024; Palli et al., 2025; Zhao et al., 2025). In the subaqueous sector of fluvial-dominated coastal systems, pollen assemblages are mainly controlled by river transport and reliably represent catchment vegetation (Brown et al., 2007), as demonstrated in the Rhône prodelta through comparison with the modern pollen rain (Beaudouin et al., 2005). Offshore, longshore currents may play a minor but significant role in shaping pollen assemblages (Mudie and McCarthy, 2006; Cacciari et al., 2024), depending on the vegetation patterns along the shoreline. In contrast, the local contribution from airborne pollen is usually considered negligible because it would be hardly possible to assess its buoyancy in an open-marine setting subject to riverine and marine currents. Onshore, within non-marine facies, the contribution of local vegetation notably represents one of the main contributors to pollen.

Among coastal systems, deltas represent exceptional stratigraphic archives, as rapid sediment accumulation enhances chronological resolution and increases the potential to resolve short-term environmental variability (Syvitski et al., 2009; Pellegrini et al., 2024).

Several Holocene deltaic records have been investigated in the Mediterranean through a bio-sedimentary approach integrating analyses of molluscs, meiofauna, and palynomorphs, including those from the Nile (Bernhardt et al., 2012; Hennekam et al., 2015; Pennington et al., 2017), Rhône (Bassetti et al., 2016; Fanget et al., 2016), Tiber (Milli et al., 2013) and Po (Correggiari et al., 2005a; Amorosi et al., 2019, 2020; Rossi et al., 2021) deltas, among others. In the Po Delta (Northern Italy), a pollen-based analysis was applied to a mixed, Holocene marine and continental succession characterized by numerous stratigraphic discontinuities (Cacciari et al., 2020, 2024).

By focusing on a relatively continuous (40-m-thick) cored stratigraphic succession from the modern *Po della Pila* delta lobe, this study aims to: (i) reconstruct the Holocene vegetation history of the Po Delta in relation to its palaeoenvironmental evolution, (ii) provide a well-resolved record of landscape-climate-human interactions over the last three millennia, taking advantage of stratigraphically expanded prodelta successions; and (iii) assess how pollen-derived signals are preserved across different depositional environments within a shallow-marine transgressive-regressive cycle, highlighting the role of facies-controlled sedimentation rates and temporal resolution.

2. Stratigraphic and environmental setting

2.1. The Po Delta

The Po Delta represents one of the largest and most dynamic deltaic systems of the Mediterranean (Maselli and Trincardi, 2013; Fig. 1). Its delta plain stretches along the western Adriatic coasts for about 120 km (Correggiari et al., 2005a) and occupies a ~ 1550 km^2 wide, flat area (Bondesan et al., 1995). The modern multi-lobe delta covers an area of about 400 km^2 (Simeoni and Corbau, 2009).

The Po Delta morphology results from the complex interplay between natural processes and increasing human influence (Maselli and Trincardi, 2013). Shoreline evolution (Fig. 1) was mainly controlled

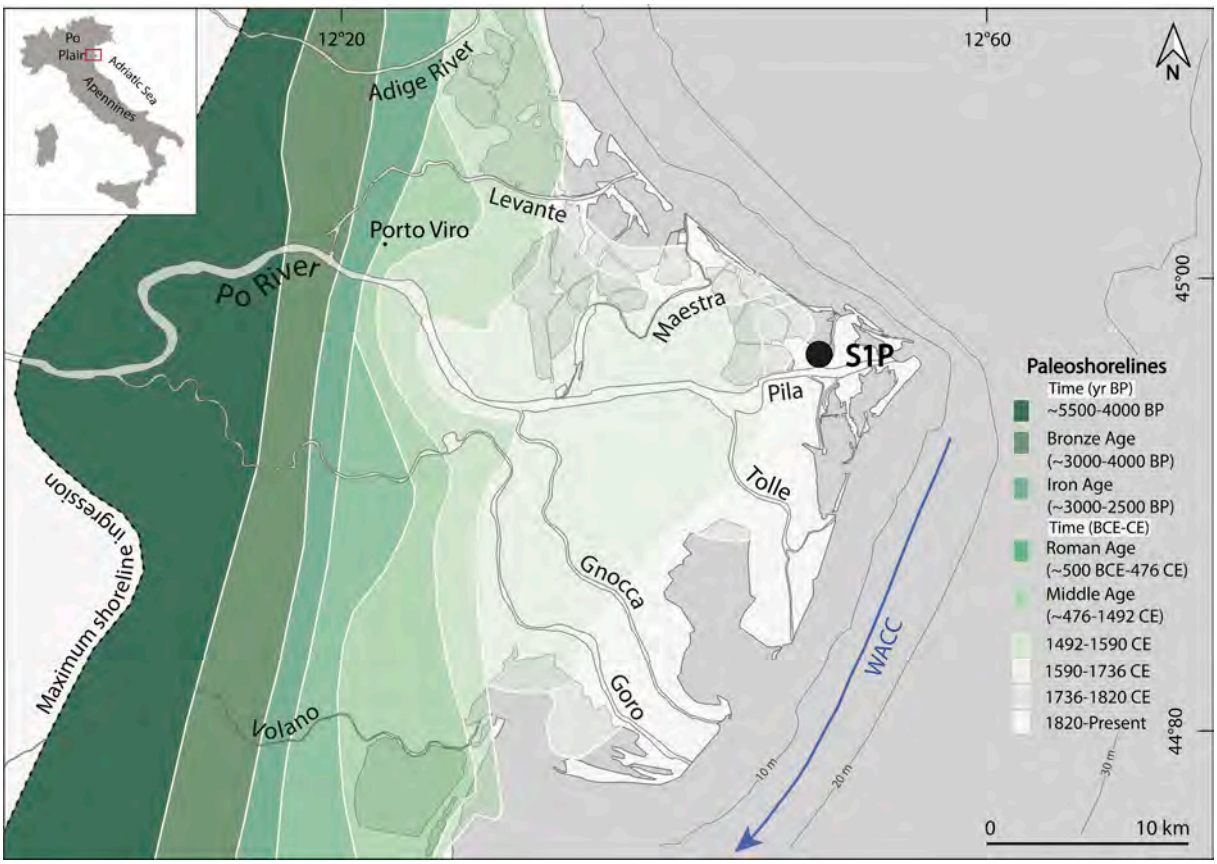

Fig. 1. Location of core S1P within the Po Delta plain. The map shows the main distributary channels and the progressive seaward migration of the shoreline following the Holocene maximum marine ingression, from the Bronze Age to the modern period. Bathymetric contours of the Adriatic shelf are shown for reference. Palaeoshorelines and the maximum marine ingression are after Correggiari et al. (2005b) and references therein; Western Adriatic Coastal Current (WACC) indication follows Artegiani et al. (1997).

by fluvial sediment supply (Nelson, 1970; Correggiari et al., 2005b; Bever et al., 2009) and secondarily by marine processes, resulting in a cuspate morphology (Galloway, 1975). The delta is fed by the 673-km-long Po River, draining a > 70,000 km^2 catchment (Trincardi et al., 2020) and delivering large water (mean discharge: 1525 m^3/s, Syvitski and Kettner, 2007) and sediment inputs to the Adriatic Sea through its five distributary channels (Fig. 1): *Po della Pila*, the main branch, accounting for 61% of water discharge and 74% of sediment load, followed by *Gnocca*, *Tolle*, *Goro*, and *Maestra,* with a progressively lower contribution (Nelson, 1970; Correggiari et al., 2005a).

Sediment delivered by the Po River generates a river plume that interacts with the northern Adriatic circulation, particularly the southward-flowing Western Adriatic Coastal Current (Vona et al., 2025). This current transports sediment alongshore for several hundred kilometers, extending beyond the Gargano Peninsula (Orlić et al., 1992; Artegiani et al., 1997; Cattaneo et al., 2003; Pellegrini et al., 2015). Plume dispersal is further influenced by Bora and Scirocco winds (Orlić et al., 1994). Marine circulation and wind regimes control sediment distribution and play a key role in the modern asymmetric progradation of Po delta lobes (Correggiari et al., 2005b).

2.2. Stratigraphy and Holocene evolution of Po Delta

The shallow subsurface stratigraphy in the Po Delta area consists of a 30 m-thick Holocene transgressive-regressive (T-R) wedge that overlies Late Pleistocene alluvial deposits. This T-R cycle consists of Early Holocene coastal to shallow-marine deposits overlain by a Middle-Late Holocene prograding deltaic system (Amorosi et al., 2008). During the Last Glacial Maximum and following Lateglacial period, the Po Delta area functioned as a wide alluvial plain. From approximately 10 kyr B.P., the river system turned into a wave-dominated estuary (Bruno et al., 2017). Relative sea level stabilized during the Middle Holocene around 7700–7000 yr B.P. (Vacchi et al., 2016), promoting the infilling of the estuarine system through prograding bay-head deltas (Amorosi et al., 2017; Bruno et al., 2017). Rapid progradation of a multi-lobe deltaic system then occurred on the shelf (Correggiari et al., 2005a). Since the Bronze Age (4250–2900 yr B.P.), the Po River discharge was dispersed through several distributary channels, forming distinct arcuate, wave-dominated deltas (Stefani and Vincenzi, 2005). Between the Recent and\or Final Bronze Age and the Middle Ages (up to 500 yr B.P.), several distributary branches of the Po River were active (Correggiari et al., 2005a). The present location of the Po Delta was established after the *Rotta di Ficarolo* (1152 CE; Veggiani, 1990), when a major flood triggered an avulsion that shifted the main channel northward to its present position. Southern distributaries progressively declined, while northern branches became dominant.

Although a significant human influence on the Po Plain started at the beginning of the Roman Period (2nd century BCE; Cremaschi et al., 1980), a strong anthropogenic imprint on the delta system became evident during the Little Ice Age (ca. 500–100 yr B.P.), when increased runoff and sediment supply, driven by wetter climate and intense upstream deforestation (Veggiani, 1990; Maselli and Trincardi, 2013; Cacciari et al., 2024), enhanced delta growth. The upbuilding of the Modern Age delta began after the artificial *Porto Viro* diversion (1600–1604 CE), a large-scale hydraulic intervention by the Venetian Republic aimed at preventing sediment infilling of the Venice Lagoon. Initially, progradation was mostly directed to the SE through the *Goro* and *Gnocca* branches, later shifting northward with the predominance of *Po di Maestra*. During the later stages of the Little Ice Age, multiple outlets coexisted, with *Po di Tolle* emerging as the main distributary. Since the 19th century, *Po della Pila* has become the dominant branch (Nelson, 1970; Correggiari et al., 2005a).

2.3. Modern climate and vegetation

The Italian Peninsula is characterized by a sub-Mediterranean climatic regime (Blasi and Michetti, 2007; Chelli et al., 2017), with the central Po Plain belonging to the continental-temperate division (Cf; Köppen-Geiger classification sensu Köppen, 1936; Kottek et al., 2006; Peel et al., 2007). The Po Delta area shows strong seasonality, with a mean annual temperature of 13.5 °C, hot and dry summers (T_{max} > 30 °C), cold and humid winters (T_{min} < 0 °C), and average precipitation of ~639 mm/yr (Soldati and Marchetti, 2017; Soboyejo et al., 2021).

The study area lies at the transition between the Central European and Mediterranean phytogeographic regions (Tomaselli, 1970; Pignatti, 1979). The Po Plain belongs to the Temperate Division (Blasi et al., 2014) and its Potential Natural Vegetation (PNV; Tüxen, 1956) is dominated by mesophilous deciduous forests (oaks and hornbeam), with hygrophilous riparian communities along river courses and black alder swamps in low-lying portions of the floodplain. Beech forests occur in the surrounding uplands of Apennine and Alpine regions. At higher elevations, coniferous forests dominated by fir, pine, and larch thrive accompanied by subalpine shrublands.

Across the Po Delta plain, vegetation follows both altitudinal and longitudinal (inland to coastal) gradients. Today, however, semi-natural vegetation covers only ~6% of the Po Plain, while the remainder is cultivated or covered by artificial surfaces (Blasi et al., 2014).

3. Materials and Methods

3.1. Sedimentary facies analysis

Borehole S1P (44°58′14.49″N; 12°29′37.49″E) was drilled about 5 km inland from the Po River mouth, near the main distributary (*Po della Pila*). The 40-m-long core was retrieved through a continuous perforating system. The core was split longitudinally and described for grain size, colour, sedimentary structures, texture, accessory components, organic matter (OM) and fossil content.

One hundred and thirty-nine samples were analyzed for the meiofauna (benthic foraminifers and ostracods) to reconstruct depositional environments in terms of water depth, salinity and organic matter. Sampling density was 3–4 samples/m in muddy intervals; substantially lower in sand layers, where the meiofauna is absent or transported/reworked. Samples were processed following the standard procedures adopted in previous Po Delta studies (Rossi and Vaiani, 2008; Barbieri et al., 2021), and the >125 μm split fraction of 41 productive samples was quantitatively analyzed. In the splitted portion, when possible, a minimum of 300 well-preserved foraminiferal tests and all ostracod valves were counted. Relative abundances were calculated separately for benthic foraminifers and ostracods. Species identification and palaeoenvironmental interpretation were based upon reference works (Ellis and Messina, 1940, 1952; Bonaduce et al., 1975; Breman, 1975; Jorissen, 1988; Athersuch et al., 1989; Sgarrella and Moncharmont Zei, 1993; Milker and Schmiedl, 2012; Jorissen et al., 2018).

3.2. Palynological analysis

Ninety-seven samples were processed for palynological studies at the "*Centro Agricoltura e Ambiente-CAA*" (Italy), following the procedures imported and adapted from the Institute of Earth Sciences, Vrije Universiteit Amsterdam (as in Lowe et al., 1996, and Cacciari et al., 2020). For each sample, 3.5–8.5 g of dry sediment were treated and a *Lycopodium* tablet was added to calculate palynomorph concentrations (grains/g). Samples were deflocculated in 10% Na-pyrophosphate, sieved (0.5 mm sieve and 5 μm filter), and chemically treated (10% HCl, acetolysis, Na-metatungstate hydrate heavy liquid, HF). Finally, following evaporation at 50–70 °C with ethanol, microscope slides were prepared with glycerol; for a detailed description of the method, see Florenzano et al. (2012). Whenever possible, 300 pollen grains per sample were recognized under 400×-1000× magnification (raw data in Catena et al., 2026 - https://doi.org/10.5281/zenodo.19252028). Identification (family, type or species) was based on morphological characteristics and

supported by atlases (Reille, 1992, 1995, 1998) and morphological keys (i.e., Andersen, 1979; Punt et al., 1984; Moore et al., 1991; Blackmore et al., 2003; Punt and Malotaux, 2007). Fern spores and selected non-pollen palynomorphs (NPPs-*Chomotriletes* sensu Van De Schootbrugge et al., 2024, dinocysts and foraminiferal linings) were also identified.

Percentages were calculated relative to the total pollen sum. Fern and Bryophyte spores were counted on the total pollen sum plus themselves (Berglund and Ralska-Jasiewiczowa, 1986). NPPs percentages were counted with respect to the pollen sum (data available in Table S1). Heavily folded or fragmented, though well preserved, grains were labeled as 'undeterminable', while those displaying corrosion and enhanced reddening (due to acetolysis) or belonging to extinct taxa were labeled as secondary, i.e., not coeval with sedimentation. Secondary and undeterminable grains were excluded from the pollen sum. Pollen concentration (grains/g) and the secondary pollen abundance were also determined.

Pollen and spores were clustered in 4 growth forms (Trees-T, shrubs-sh, Lianas-L, and Herbs-H) and 12 ecological groups (EGs) based on their ecological preferences, validated against modern regional vegetation (Pignatti et al., 2017–2019) and cluster analysis (section 3.3). Growth forms and ecological spectra were calculated for each sample and plotted against stratigraphy.

3.3. Statistical analyses

To evaluate the robustness of the ecological grouping adopted in this study, an unconstrained hierarchical cluster analysis (UPGMA, Pearson's r similarity measure) was performed on the pollen taxa matrix, following the methodologies of Tarasov et al. (1998), Kaniewski et al. (2011), and Cacciari et al. (2020).

The dataset was standardized by aggregating taxa with similar ecological affinities, combining herbaceous taxa at the family level and, where appropriate, arboreal taxa at the genus level, in order to reduce the noise. Rare taxa (maximum abundance <1% and occurrence in fewer than ~10% of samples) were excluded from the analysis and grouped as *alia* (only the herbaceous component); among 97 samples, one was excluded because of a pollen sum <100 grains (Table S2).

Subsequently, pollen zones (PZs) were defined independently via cluster analysis to identify hierarchical groupings based on vegetation similarity among samples (96 out of 97). This analysis was performed using CONISS (Constrained Incremental Sum of Squares; sensu Grimm, 1987), maintaining the stratigraphical order of samples within the succession. The input matrix retained the percentages of each ecological group, with chestnut separated as an individual sub-group from the other cultivated taxa. The cluster analyses were conducted in PAST v. 4.03 (Hammer et al., 2001).

To assess the relationship between vegetation dynamics and climate variability, an additional analysis was performed by comparing peaks in montane taxa with independently defined cold phases based on the 2500-year-long European temperature reconstruction of Büntgen et al. (2011), in which multi-decadal intervals of sustained negative temperature anomalies were evaluated in the context of well-known historical climatic deteriorations. Given the remarkable distance of the core site from the reliefs (more than 50 km), montane taxa are considered a reliable proxy for cooling events. The temporal correspondence between montane peaks and negative temperature anomalies was quantified, and its statistical significance was assessed using a Monte Carlo approach, in which peak positions were randomly redistributed within the considered time interval to test whether the observed correspondence exceeded that expected by random chance.

3.4. Dating and chronology

The chronology was reconstructed through: (i) AMS ^{14}C analysis of 7 samples (Table 1) conducted at NOSAM laboratory; (ii) ^{210}Pb and ^{137}Cs radionuclides activity analysis of 14 samples (Fig. S1; Table S3), treated at CNR-ISMAR laboratories, following standard procedures described by Frignani et al. (2004) and Bellucci et al. (2007).

For radiocarbon, conventional ages were calibrated differentiating terrestrial, marine or mixed organic reservoirs, based on the type of organic material. Five samples consisting of terrestrial organic matter (wood fragments or peat) were calibrated using the IntCal20 curve (Reimer et al., 2020). The remaining two samples, derived from river-influenced marine deposits, were calibrated using the Mixed Northern Hemisphere curve (Heaton et al., 2020), assuming a 50:50 mixture of marine and terrestrial organic matter (Table 1).

^{137}Cs is a product of nuclear fission that accumulates in sediments as distinct peaks, corresponding to the 1963 maximum fallout from atmospheric nuclear testing and the 1986 Chernobyl fallout. Initial deposition in sediments in 1954 (onset of nuclear bomb testing) can also be traced. ^{210}Pb dating is effective in stable environments with relatively uniform accumulation rates (Appleby, 1998), allowing reliable age estimates for sediments up to 100 year old (Swarzenski, 2014).

To refine chronology, an age-depth model was computed through RStudio (R v.4.5.1), using the package rBacon (v. 3.5.2), which reconstructs accumulation histories for deposits using Bayesian Statistics (Blaauw and Christen, 2011; Fig. S2). In addition to radiometric dates, also stratigraphic features were used to further constrain the model. The model runs millions of iterations to generate weighted mean age estimates at 5 cm intervals, representing the highest achievable resolution for the dataset.

4. Results

4.1. Core stratigraphy

Based on the integration of sedimentological and meiofaunal data, six facies associations were identified along core S1P (Fig. 2). They are described in ascending order.

4.1.1. Open-bay facies association (40–36.97 m)

Description.

This facies association, approximately 3 m thick, consists of grey muds with silty sand intercalations and abundant organic matter, including cm-thick, silt to silty-sand layers enriched in organic matter, vegetal remains and thin peat layers. Bioturbation and shell fragments are common. Foraminifers are dominated by OM-sensitive, epiphytic species (up to ~45%), mainly *Buccella granulata* (~3–28%), *Neoconorbina terquemi* (~2–14%) and *Asterigerinata mamilla* (~2–11%), with secondary OM-opportunistic species including *Porosononion granosum* (~5–18%), *Ammonia tepida* (~2–17%), and *Aubignyna perlucida* (~2–12%). Ostracods are scarce, mainly littoral *Cushmanidea turbida*, accompanied by marine (e.g., *Sagmatocythere napoliana*, *Semicytherura* species) and euryhaline, brackish-marine taxa (*Cyprideis torosa*, *Xestoleberis communis*, *Leptocythere bacescoi*). This facies is constrained by three radiocarbon dates: 10681–10,370, 10250–10,122, and 9827–9553 cal yr B.P.

Interpretation.

Sedimentological and faunal evidence indicate deposition in a back-barrier environment with vegetated bottoms and a high seawater exchange, likely an open bay partially confined by sandy spits or coastal barriers. These conditions promoted the accumulation of organic matter and plant remains, as well as the development of suitable conditions for opportunistic foraminifers and euryhaline, brackish-marine ostracods.

4.1.2. Transgressive-barrier facies association (36.97–36.77 m)

Description.

This facies association consists of thin (~20 cm) fine sand, with abundant mollusc fragments, underlain by an erosional surface. The sand is massive at the base and slightly laminated at the top. Foraminifers are dominated by hyaline epiphytic species sensitive to organic-

Table 1
Chronological dates implied for the S1P age-depth model based on radiocarbon dating (AMS ^{14}C) and short-lived radionuclide activity.

Sample depth (m)	Dating method	Measured activity/ conventional age	Material	Assigned Age [cal. yr B.P. (2σ) or CE]	Chronological reference/calibration
2.10	^{137}Cs	13.14 ± 0.87 Bq/kg	Sediment	1986 CE	Chernobyl fallout peak
3.41	^{137}Cs	5.07 ± 0.95 Bq/kg	Sediment	1954 CE	Onset of nuclear weapons testing
5.24	^{210}Pb	supported Pb = ~17 Bq/kg	Sediment	1920 CE	Pb equilibrium depth
21.65	^{14}C AMS	385 ± 15 yr B.P.	Plant/wood	497–442 cal. yr B.P.	IntCal20
27.75	^{14}C AMS	2.080 ± 20 yr B.P.	Organic mud	1867–1688 cal. yr B.P.	50% IntCal-50% Marine
35.65	^{14}C AMS	6.210 ± 35 yr B.P.	Organic mud	6903–6629 cal. yr B.P.	50% IntCal-50% Marine
37.80	^{14}C AMS	9.220 ± 45 yr B.P.	Peaty sediment	10,504–10,249 cal. yr B.P.	IntCal20
37.95	^{14}C AMS	8.740 ± 45 yr B.P.	Peaty sediment	9827–9553 cal. yr B.P.	IntCal20
39.73	^{14}C AMS	9.020 ± 45 yr B.P.	Organic mud	10,250–10,122 cal. yr B.P.	IntCal20
39.95	^{14}C AMS	9.320 ± 50 yr B.P.	Organic mud	10,681–10,370 cal. yr B.P.	IntCal20

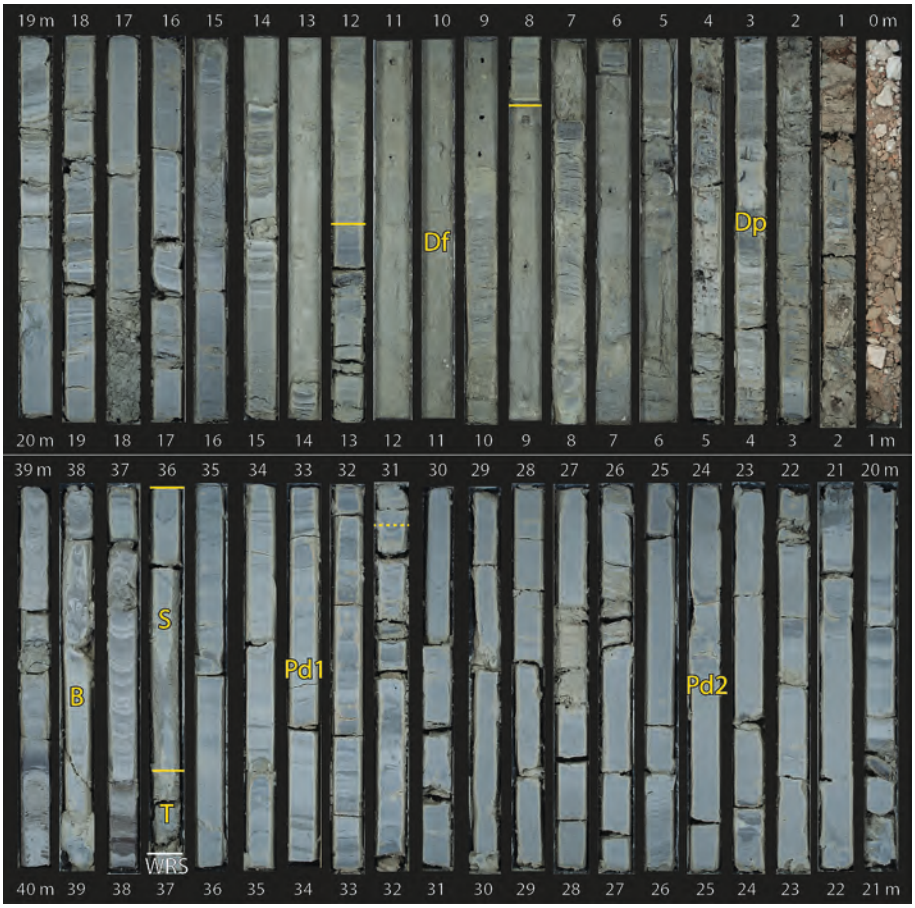

Fig. 2. Core photographs illustrating the facies associations and lithofacies recognized along core S1P. B: open bay; T: transgressive barrier; S: inner shelf; Pd1-Pd2: prodelta deposits; Df: delta front; Dp: delta plain; WRS: wave ravinement surface. Depth (m) is indicated along the core boxes.

enrichment (up to ~50%), including *B. granulata* (~14%), *N. terquemi* (~11%), *Lobatula lobatula* (~6%), and miliolids (~20%). Opportunistic foraminifers are mainly *P. granosum* (~11%), while the sparse ostracod fauna is poorly diversified, with dominant *C. turbida* and minor occurrences of *S. napoliana* and *Cytheretta subradiosa*.

Interpretation.

The thin, bioclast-rich sand above an erosional surface indicates a high-energy coastal environment, interpreted as a transgressive barrier. This interpretation is supported by the presence of a shallow-marine meiofauna, dominated by sensitive, mainly epiphytic foraminifers with few littoral-sublittoral ostracods thriving in highly mobile substrates (Bonaduce et al., 1975; Barbieri et al., 2021). The erosional surface is interpreted as a wave ravinement surface (Nummedal and Swift, 1987) that truncates the underlying bay deposits, marking shoreline retreat during transgression.

4.1.3. Inner-shelf facies association (36.77–36.00 m)

Description.

This facies association, ~80 cm thick, consists of soft silty clay, with occasional (~2 cm) fine sand-silt interbeds. The meiofauna is slightly more diversified than in underlying transgressive-barrier deposits, representing the richest community of the whole cored succession. OM-sensitive species, including abundant hyaline and miliolid epiphytic species, such as *B. granulata* (~18%), *N. terquemi* (~10%), and *Siphonaperta aspera* (~4%) remain dominant (~50%). The association also includes OM-indifferent and OM-opportunistic foraminifers (*Ammonia beccarii*, *Haynesina depressula*, *Quinqueloculina seminulum*, *P. granosum* and *A. perlucida*).

Interpretation.

Fine-grained deposits and meiofaunal assemblages indicate a shallow-marine environment (~20–40 m deep) covered by vegetation and subject to moderate OM fluxes. These features are consistent with a low fluvial-influenced inner shelf, comparable to the present North Adriatic sediment-starved area updrift of the Po River mouth (Barbieri et al., 2019).

4.1.4. Prodelta facies association (36.00–12.50 m)

Description.

This facies association, ~24 m thick, comprises two facies (Pd1 and Pd2) stacked in an overall coarsening-upward trend. The stratigraphic surface that separates these two facies documents a major change in the meiofauna. Three radiocarbon dates constrain this interval: 6903–6629 cal yr B.P. (35.65 m), 1867–1688 cal. yr B.P. (27.75 m), and 497–442 cal. yr B.P. (21.65 m), respectively.

Facies Pd1 (36.00–31.10 m) consists of light grey, soft clay, with mm-thick silt and sand intercalations, and typically containing shell fragments. The meiofauna shows a marked turnover from the underlying inner-shelf muds, with an abrupt increase in OM-opportunistic taxa (up to ~80%), mainly *A. perlucida* (~3–44%), *Q. seminulum* (~3–40%), *A. tepida* (~5–28.5%) and *P. granosum* (~5.5–19%). Sensitive epiphytic species are largely reduced, but locally peak (40–55%). Ostracods are rare and include *C. turbida*, *S. napoliana*, *C. subradiosa*, *Leptocythere* and *Semicytherura* species.

Facies Pd2 (31.10–12.50 m) is ~18.5 m thick and consists of dark grey, soft silty clay, with thicker (mm- to dm) silt and sand layers, especially abundant in its upper portion, with an overall coarsening-upward and thickening-upward trend. It is marked at the base by the occurrence of degassing features, and a strong decline in meiofauna abundance. Wave ripples and bioturbation occur only locally. The meiofauna is very scarce, almost entirely composed of opportunistic foraminiferal species (*A. tepida*, *A. perlucida,* and *P. granosum*). Ostracods are nearly absent.

Interpretation.

Alternating clay and silt/sand layers, together with a relatively diversified foraminiferal fauna dominated by opportunistic species, indicate deposition of this facies association in a prodelta environment (Amorosi et al., 2019; Rossi et al., 2021). The scarcity of ostracods likely reflects the high sediment supply typical of prodelta settings (Barbieri et al., 2019, 2021; Scarponi et al., 2022).

Facies Pd1 closely resembles the one that thrives on the modern north-central Adriatic mud wedge around 15–25 m water depth (Barbieri et al., 2019). The local record of sensitive species is interpreted to reflect a greater activity of marine (longshore) processes in shaping and nourishing the seabed.

Facies Pd2 records more stressful conditions, marked by a sharp decline in the meiofauna and dominance of opportunistic foraminifers, likely due to high sediment accumulation via river fluxes. Degassing features further support rapid sedimentation, as gas becomes trapped during fast mud accumulation (e.g. García-García et al., 2007). Overall, Pd2 reflects a prodelta increasingly influenced by river plumes. This interpretation is supported by the pronounced upward coarsening and thickening trend of sandy beds, marking the approach of the river mouth (Gamberi et al., 2020).

4.1.5. Delta-front facies association (12.50–8.10 m)

Description.

This facies association displays a general coarsening-upward trend and consists predominantly of amalgamated fine sand layers, normally graded and containing bioclasts, mica, and plant remains. Silt interbeds with parallel lamination occur between sandy units. The faunal content is extremely scarce, limited to a few reworked benthic and planktonic foraminifers. The base of this facies association, at 12.50 m depth, is marked by the occurrence of thick, amalgamated sand bodies.

Interpretation.

The dominance of fine sands, the near absence of fossils, and stratigraphic relations with the underlying prodelta deposits, indicate deposition under high-energy conditions and rapid sediment accumulation, consistent with a delta front environment (Amorosi et al., 2017; Scarponi et al., 2022).

4.1.6. Delta-plain facies association (8.10 m-top)

Description.

The uppermost ~8 m of the stratigraphic succession consist of dark grey, very soft and organic-rich muds, with abundant wood fragments and terrestrial plant remains, locally interbedded with silty-sand layers. The faunal content is scarce, with poorly preserved foraminifers and scattered valves of brackish to hypohaline ostracods, mainly *Cyprideis torosa* and *Candona* species.

Interpretation.

This facies association accumulated in an interdistributary area of the modern Po Delta plain. The fine-grained, organic-rich muds indicate low-energy conditions, vegetated environments, and episodic river flooding recorded by sandy interbeds. The occurrence of brackish-hypohaline ostracods further supports deposition in a slightly brackish setting.

4.2. Chronology and accumulation rates

Chronology and sediment accumulation rates (SARs) for core S1P were reconstructed by integrating radiocarbon and short-lived radionuclide dating (Table 1) with stratigraphic constraints derived from facies analysis, resulting in a robust age-depth model. Of the seven ^{14}C AMS samples analyzed, six yielded reliable results, whereas one (37.80 m depth, Table 1) showed an age inversion and was excluded from the model.

Key stratigraphic surfaces, corresponding to stratigraphic unconformities and major facies boundaries, were used to constrain the model, and SARs were calculated for the intervening stratigraphic intervals (Fig. 3).

Throughout the manuscript, chronological data related to the sedimentary succession and pollen zones are expressed as calibrated years B.P. (cal yr B.P.), whereas the CE notation is retained for historically documented climatic phases and events.

According to the model, the open-bay deposits (up to 36.95 m) record low SARs (~0.14 cm/yr). The erosional ravinement surface at the base of transgressive-barrier sands marks a hiatus of ~1000 years. Above this surface, SAR slightly drops to ~0.11 cm/yr within prodelta deposits. At 31.00 m depth, the Pd1-Pd2 boundary corresponds to a short-lived hiatus. Above this surface, SAR progressively increases to ~0.5 cm/yr, between 31 m and 19.70 m. At this stratigraphic level, dated to shortly after ~500–450 cal yr B.P. (ca. 1450–1500 CE), an increase in the sand proportion within prodelta deposits is associated with significantly higher SARs (2.94 cm/yr). At 12.50 m depth, the Pd2-Df boundary marks the base of delta-front deposits, developed around ~130 cal yr B.P. (ca. 1820 CE). Above this boundary, accumulation rates peak at 7.79 cm/yr and persist up to 2.10 m, the stratigraphic level of the youngest dated sample.

Short-lived radionuclide data provide independent chronological constraints for the uppermost delta-plain deposits. The ^{210}Pb activity reaches equilibrium (17.5 ± 2.4 Bq/kg) with supported values of 17.0 Bq/kg at 5.24 m depth, corresponding to ~100 yr B.P. ^{137}Cs profiles show an initial signal at 3.41 m depth (5.07 ± 0.95 Bq/kg), likely related to the onset of atmospheric nuclear weapons testing at 1954 CE, and a distinct peak at 2.10 m depth (13.14 ± 0.87 Bq/kg), attributed to the 1986 Chernobyl fallout, consistent with previous data from the Po Delta area (Frignani et al., 2004).

4.3. Pollen groups (EGs)

To support the definition of ecological groups, four main pollen-

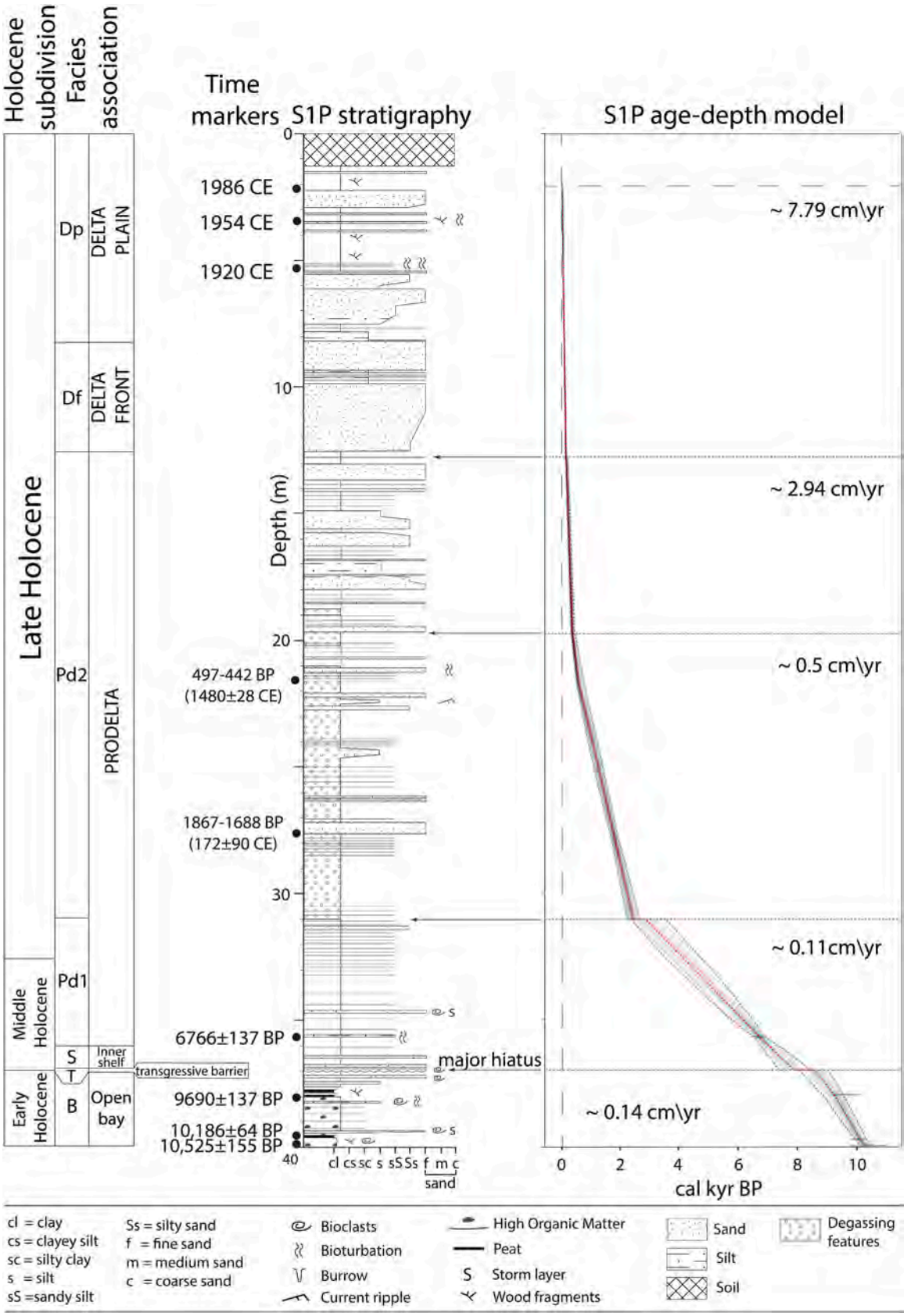

Fig. 3. Stratigraphy and age-depth model of core S1P. The left panel shows the vertical stacking pattern of facies associations identified along the core together with stratigraphy and dates used to refine the age model. The right panel displays the age-depth model together with the average sediment accretion rates, reported for each interval.

derived biomes (PDBs; Fig. 4A) were identified through unconstrained cluster analysis. The identified PDBs include: (i) a swamp-forest assemblage, grouping black alder with hygrophilous and aquatic taxa typical of wetland environments; (ii) a riparian oak-willow forest assemblage, characterized by meso-hygrophilous arboreal taxa representative of alluvial plain woodlands; (iii) a semi-anthropised meso-hygrophilous grassland assemblage, including cultivated trees and herbs, disturbance indicators, and open-land ubiquists herbs; and (iv) a conifer forest assemblage with xero-hygrophilous grasslands, dominated by conifers associated with dry, halophilous and open-land taxa.

At the highest ecological distance, the dendrogram primarily reflects a moisture gradient, ranging from wetland and riparian environments to open and relatively dry vegetation communities. Because vegetation composition changed substantially throughout the Holocene succession, these assemblages should not be interpreted as discrete vegetation types, but rather as groups of taxa that tended to increase or decrease together under similar environmental conditions. For this reason, the twelve ecological groups (EGs) adopted in this study integrate cluster results with present-day regional vegetation physiognomy and the ecological preferences of the identified taxa, following the floristic classification of Pignatti et al. (2017–2019). The EGs are described in detail in Table 2, showing a strong similarity with those previously established for the Po Plain by Cacciari et al. (2020).

However, montane taxa show a more complex distribution and are partially dispersed among different biomes. To further investigate the ecological relationships among montane taxa, an additional cluster analysis was performed specifically on these (Fig. 4B). This analysis identified three main assemblages corresponding to conifer forests, hygrophilous montane woods, and beech forests respectively. This distinction supports the palaeoenvironmental interpretation of montane vegetation dynamics implied in this study.

4.4. Pollen zones

A total of 32,219 palynomorphs were identified, comprising pollen, fern spores, bryophytes, and secondary grains. Specifically, 28,072 pollen grains were assigned to 172 taxa (64 arboreal and 108 herbaceous), 1215 fern spores to 15 taxa, 87 bryophyte spores to 3 taxa and 2845 secondary grains to 14 taxa. Additionally, 223 specimens of *Chomotriletes* and 463 dinocysts were recognized. Pollen concentration varies considerably, from ~1000 grains/g to 127,000 grains/g, with higher values at the base and top of the sequence. Secondary pollen also shows a marked variability along the core. Despite marked variability in pollen concentration, nearly all samples yielded sufficiently abundant palynomorphs for palaeoecological interpretation; samples with lower concentrations were counted until at least 100 pollen were reached. Only one sample with <100 grains was excluded from palaeoecological interpretation and statistical analyses (see section 3.3).

4.4.1. PZ1 (40–39.65 m; ~10.5 to ~10.2 cal kyr B.P.)

PZ1 is a thin pollen zone corresponding to the lowermost open-bay deposits. Pollen concentrations are very high (11-65 k/g) and secondary grains are absent or rare. Afforestation is low (22–32%, Fig. 5), as the landscape is characterized by an open wooded grassland dominated by spontaneous Poaceae, Cichoriae, and Asteroideae (pm ~43–53%, Fig. 5), with subordinate wetlands composed of Cyperaceae, ferns, *Sparganium*, *Potamogeton*, and *Nymphaea* (hyg + hel + hyd ~18%). Forested areas are limited to scattered shrublands of *Quercus*, *Salix*, and *Corylus* (Q + I ~ 10–25%). Montane forest taxa are subordinate (Mt ~4–13%) and mainly represented by *Pinus*, locally accompanied by *Betula*, *Abies*, and *Fagus* (Fig. 6). Rare taxa are scarce, including halophytes (hal <2%) (e.g., *Artemisia*, Amaranthaceae, Fig. 7) and indicators of disturbed environments (As <2%) (e.g., Caryophyllaceae); cultivable taxa are negligible (<2%), except at 38.49 m depth, where *Castanea* and *Juglans* each reach ~3% (Fig. 8).

4.4.2. PZ2 (39.65–37.65 m; ~10.2 to ~9.2 cal kyr B.P.)

PZ2, within the open-bay facies association, shows high pollen concentrations (8-127 k/g) and low secondary pollen (<3%). Afforestation is medium-high (T + sh + L ~ 50%), with two peaks at ~80% (Fig. 5). PZ2 records a marked vegetation shift from PZ1, with strong afforestation by deciduous oak forests (Q = 36.6%) and montane taxa (Mt = 27.3%, Fig. 5). Oak forests largely consist of hazel woodlands (*Corylus* = 26.3%, Fig. 6), while *Pinus*, *Alnus incana* and *Abies* make up most of the montane component; hygrophilous trees, especially *Alnus glutinosa* (H = 12.5%), are also significant. Upsection, mesophilous and hygrophilous grasslands shrink (pm ~13%; hyg + hel + hyd ~11%), whereas true oak forests dominate (Q ~ 20–40%) alongside a first significant increase in Mediterraneans (M ~ 3%–10%); montane forests also increase (Mt ~12%). Mesophilous grasslands range between ~25% and ~ 45%, whereas the hygrophilous component is represented by herbaceous hyg + hel + hyd (~14%- ~ 20%): two organic-rich layers display peaks in hydrophytic taxa, particularly *Sparganium* (~4–6%, Fig. 7). The uppermost PZ2 shows a marked peak in mixed oak woods (Q ~ 40%, Fig. 5), mainly represented by *Corylus* (Fig. 6), and a concurrent increase of the hygrophilous tree (H ~ 25%) *A. glutinosa* (Fig. 6). Montane trees remain stable, whereas Mediterraneans slightly decline and meso-hygrophilous grasslands significantly decrease (pm ~7%; hyg + hel + hyd ~6.5%).

4.4.3. PZ3 (37.65–27.40 m; ~9.2 to ~1.7 cal kyr B.P.)

PZ3 is a very thick pollen zone spanning multiple facies associations (open-bay muds, transgressive-barrier sands, inner-shelf muds, and lowermost prodelta deposits). Pollen concentrations range from 1.3 to 12.2 k/g, whereas secondary pollen percentages vary between 1.4% and 11.4%, with a slight upward increase in absolute concentrations from ~32 m. PZ3 is subdivided into four subzones (3a-3d).

PZ3a (37.65–35.00 m; ~9.2 to ~ 6.2 cal kyr B.P.)

PZ3a encompasses the coastal-shallow marine transition and extends into the lowermost prodelta muds (facies Pd1). Its lower part includes the wave ravinement surface. Subzone 3a marks a major shift to a mature forested landscape dominated by *Q. pubescens* and *Q. cerris* (Q ~ 16%–31%), peaking in the uppermost part and indicating maximum forest maturity (PNV). The arboreal hygrophilous component (H ~ 4–14%), consisting of *Salix* and *Alnus*, is subordinate to the mesophilous oak wood. The Mediterranean component is scarce (M < 4%) and shows a further decline toward the top of the subzone. However, forests do not consist of a thick and uniform canopy: extensive mesophilous grasslands with spontaneous Poaceae and Cichorieae (pm ~19–35%), and subordinate wetlands (hyg + hel + hyd ~17–29%), mainly colonized by Cyperaceae, are consistently present. Montane taxa, mostly *Pinus*, are relatively low (Mt ~7.5–11%) but show two major peaks at the bottom and at the top (~Mt. = 22%, Fig. 5) dated to ~9.2 kyr B.P. and ~ 6.3 kyr B.P., respectively. The lower peak is associated to abundant montane alder and birch, whereas *Abies* is more representative of the upper peak (Fig. 6). Cultivated taxa, mainly cultivated trees represented by *Castanea* and *Juglans*, appear (Cc ~3–7.5%, Fig. 8) and become abundant toward the top of the subzone. A significant increase in cereals, only sporadically observed in older deposits, is recorded at 37.10 m (*Avena-Triticum* = 2.3%, Fig. 8). Indicators of disturbed environments, such as *Plantago* and Caryophyllaceae, display notable fluctuations (As ~1.7–8.8%).

PZ3b (35.00–31.80 m; ~6.2 to ~ 3.4 cal kyr B.P.)

PZ3b develops entirely within prodelta facies Pd1. Afforestation is medium-high (T + sh + L ~ 44- ~ 60%, Fig. 5), with lower values near the base. The vegetation is dominated by meso-hygrophilous forests composed of *Q. pubescens*, *Salix*, *Alnus*, and *Humulus lupulus* (Q ~ 14–24%; H ~ 7.5–18%). The Mediterranean component is scarce but shows a slight upward increase (M ~ 1–7%). Mesophilous grasslands dominated by wild Poaceae and Cichorieae (pm ~11–27%) are present along with subordinate wetlands composed of Cyperaceae, *Sparganium*, *Hydrocharis* and other hydrophytes (hyg + hel + hyd ~10–21%). Cultivated taxa are constantly observed (Cc ~3.6%–8%), mainly

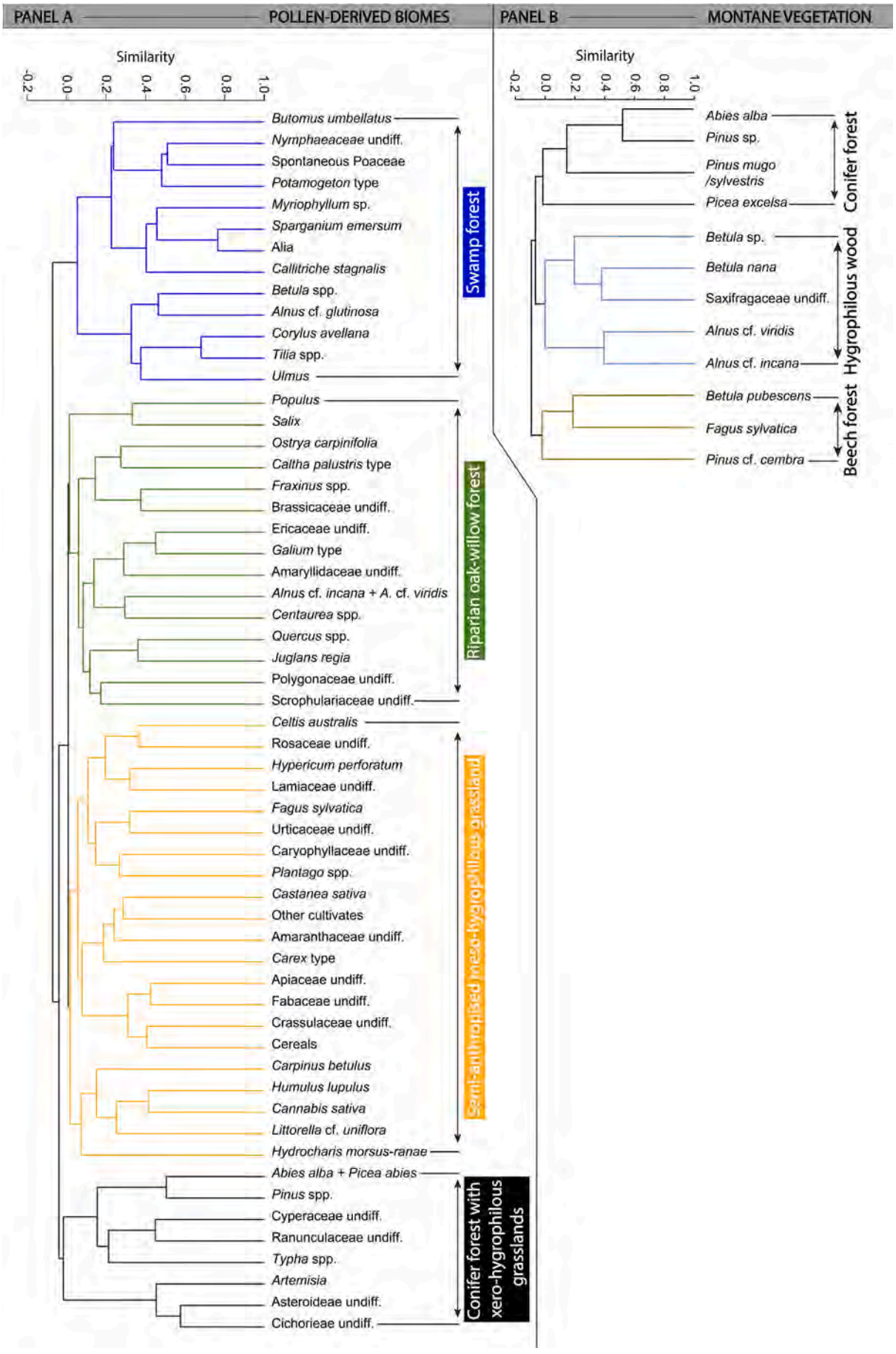

(caption on next page)

Fig. 4. Hierarchical cluster analysis of pollen taxa showing the main pollen-derived biomes (PDBs) identified in the S1P record. Panel A: cluster analysis performed on the full pollen taxa matrix highlighting four main assemblages: (i) swamp forest, (ii) riparian oak–willow forest, (iii) semi-anthropised meso-hygrophilous grassland, and (iv) conifer forest with xero-hygrophilous grasslands. Panel B: cluster analysis performed on a reduced matrix including only taxa with montane affinity, identifying three main assemblages: (i) conifer forest, (ii) hygrophilous montane forest, and (iii) beech woods.

Table 2
Ecological groups (EGs) identified in core S1P, with their principal representative taxa and associated ecological value.

Ecological group		Principal taxa	Ecological value
Montane taxa	(Mt)	*Alnus incana*, *Alnus viridis*, *Betula* spp., *Fagus sylvatica*, *Abies alba*, *Pinus* spp., Saxifragaceae.	Trees and herbs of the subalpine woods.
Mixed oak forest	(Q)	*Carpinus betulus*, *Corylus avellana*, *Ostrya carpinifolia*, *Cornus* spp., *Quercus cerris*, *Q. pubescens*, *Q. robur*, *Fraxinus* spp., *Acer campestre*, *Ulmus*.	Deciduous temperate trees of the mesophilous woods.
Mediterraneans	(M)	*Buxus*, *Cistus*, *Helianthemum*, *Quercus ilex*, *Myrica*, *Olea europaea*, *Phillyrea*, *Pinus halepensis*.	Sclerophyllous taxa of the thermophilous woods.
Woody hygrophytes	(I)	*Alnus glutinosa*, *Humulus lupulus*, *Populus*, *Salix*.	Humid and riparian taxa of hygrophilous woods.
Herbaceous hygrophytes	(hyg)	*Carex*, other Cyperaceae, Juncaceae, *Caltha palustris*, ferns.	Herbs of hygrophilous grasslands.
Helophytes	(hel)	*Butomus umbellatus*, *Phragmites australis*, *Sparganium erectum*, *Typha* spp., *Isoetes*.	Partially or seasonally submerged aquatic plants.
Hydrophytes	(hyd)	*Myriophyllum*, *Hydrocharis*, *Nymphaea* spp., *Callitriche*, *Litorella uniflora*, *Potamogeton*, *Sparganium emersum*, *Salvinia natans*.	Fully aquatic plants.
Pastures and meadows	(pm)	Asteroideae, Cichorieae, Fabaceae, wild Poaceae.	Herbaceous plants of open mesophilous grasslands.
Halophytes	(hal)	Amaranthaceae, *Artemisia*, *Plantago maritima*.	Salt-tolerant species of coastal or saline environments.
Spontaneous anthropic	(As)	*Centaurea* spp., *Xanthium*, Caryophyllaceae, Convolvulaceae, Papaveraceae, *Plantago* spp., *Polygonum* spp., *Rumex*, *Verbascum*, Urticaceae.	Disturbance-adapted species, likely of anthropized habitats.
Ubiquists	(u)	Amaryllidaceae, Apiaceae, Boraginaceae, Brassicaceae, Crassulaceae, Ranunculaceae, Rubiaceae, *Sanguisorba minor*, Scrophulariaceae.	Taxa with broad habitat tolerance.
Cultivates	(Cc)	*Castanea sativa*, *Juglans regia*, *Vitis*, *Cannabis sativa*, *Avena-Triticum* group, *Hordeum* group/type, *Triticum*, *Zea mays*.	Plants present in the wild and domesticated for cultivation.

Castanea and *Juglans*, along with occasional *Cannabis* (Fig. 8). The montane component is relatively low (Mt ~6.6%–15%) and represented by *Pinus*, *Fagus*, *Alnus viridis,* and *Betula*, with a slight increase in the middle part of the subzone.

PZ3c (31.80–31.00 m; ~3.4 to ~ 2.8 cal kyr B.P.)

A meso-hygrophilous forest, variably dominated by *Q. pubescens*, *Alnus*, *Salix*, *Corylus* (Q ~ 12–22%; H ~ 4–15%) characterizes uppermost prodelta facies Pd1. Extensive mesophilous grasslands are mainly composed of spontaneous Poaceae and Cichorieae (pm ~20–27%), with subordinate wetlands (hyg + hel + hyd ~10–18%) colonized by Cyperaceae and ferns. Indicators of disturbed environments, halophilous taxa (Amaranthaceae and *Artemisia,* Fig. 7), and cultivated taxa (Cc ~3.5–8%) are minor components that decline upward. The Mediterranean vegetation is generally scarce, except at the base (~6–1%). The montane component is variable (Mt ~11–20%) and represented by *Pinus*, *Abies*, *Fagus*, *Alnus*, and *Betula*, with two marked peaks in *Pinus* and *Abies* and a concurrent decline in hygrophilous trees (Fig. 7).

PZ3d (31.00–27.40 m; ~2.4 to 1.7 cal kyr B.P.)

PZ3d, at the base of prodelta lithofacies Pd2, is generally characterized by a meso-hygrophilous forest dominated by *Q. pubescens* and *Q. robur* (Q ~ 9–25%), accompanied by *Alnus*, *Salix*, and *H. lupulus* (H ~ 8–15%), with occasional *Corylus*. The Mediterranean component fluctuates (M ~ 1–7.7%). Well-developed mesophilous grasslands consist primarily of spontaneous Poaceae, Cichorieae, and Asteroideae (pm ~14.5–22%). Wetland vegetation is dominated by Cyperaceae, ferns, and hydrophytes, such as *Hydrocharis* and *Myriophyllum* (hyg + hel + hyd ~12–25%). Halophytes (e.g., Amaranthaceae, Fig. 7) and As taxa slightly increase toward the top. Cultivated taxa are present throughout (Cc ~3–13%), with peaks in *Castanea sativa* at the base (~9%, Fig. 8) and toward the top of the subzone, the latter being associated to a noticeable percentage of cereals (*Avena-Triticum* ~ 2%, Fig. 8). High-altitude trees show a slight increase relative to the underlying subzone (Mt ~8–25%, Fig. 5) and *Fagus* is progressively replaced upward by *Pinus* and *Abies* (Fig. 6).

4.4.4. PZ4 (27.40–15.60 m; ~1700–225 cal yr B.P.)

PZ4 largely corresponds to prodelta facies Pd2. Pollen concentration is low-medium (0.8-7 k/g), while secondary pollen percentages are generally high (>7%), peaking at ~22%. PZ4 is subdivided into four subzones (4a-4d).

PZ4a (27.40–23.00 m; ~1700–950 cal yr B.P.)

PZ4a develops on locally laminated muds with degassing features. Pollen composition is relatively homogeneous, with major changes in montane and cultivated taxa. Afforestation is lower at the base (T + sh + L ~ 44%, Fig. 5), then rising to constant values (~50%). The dominant vegetation is a meso-hygrophilous shrubland composed by *Q. pubescens*, other deciduous oaks, *A. glutinosa*, *Salix*, *H. lupulus*, *Ulmus*, *Corylus*, and rare *Fraxinus* spp. (Q ~ 10–15%; H ~ 6–17%). Mesophilous grasslands are widespread, rich in spontaneous Poaceae, Cichorieae, and Asteroideae (pm ~19–28%). Subordinate wetlands consist of Cyperaceae, *Carex* spp., and ferns (hyg + hel + hyd ~14–20%). Disturbance indicators, mainly *Plantago* spp., are stable or slightly increasing, while halophytes (Amaranthaceae) are constant. Cultivated taxa are constant at the base, decrease in the middle, and rise again upwards (Cc ~5–10%). Montane species, particularly *Pinus* and *Abies*, increase at the base, slightly decline upwards, and stabilize toward the top (Mt ~8–16%).

PZ4b (23.00–20.40 m; ~950–450 cal yr B.P.)

PZ4b encompasses muds with degassing features, locally interbedded with sand layers. Afforestation is medium-high (T + sh + L ~ 42–58%, Fig. 5). Vegetation is dominated by meso-hygrophilous forests and shrublands composed of *Q. pubescens*, *Salix*, *Alnus*, *H. lupulus*, *Corylus*, and *Ulmus*, with occasional *Fraxinus* spp. Deciduous oak forests remain stable, while hygrophilous trees slightly decline upward (Q ~ 12–19%; H ~ 5–16%). Mediterraneans are consistently present (M ~ 2–5%). Extensive mesophilous grasslands include spontaneous Poaceae and Cichorieae (pm ~15–29%). Wetlands are subordinate and slightly decreasing toward the top (hyg + hel + hyd ~12–20%). As taxa are stable or increasing, dominated by *Plantago* and Caryophyllaceae. Halophytes are well represented at the base (hal ~1–5%), but decline toward the top, except for a peak at 20.72 m (~9%, Fig. 5). Cultivated taxa

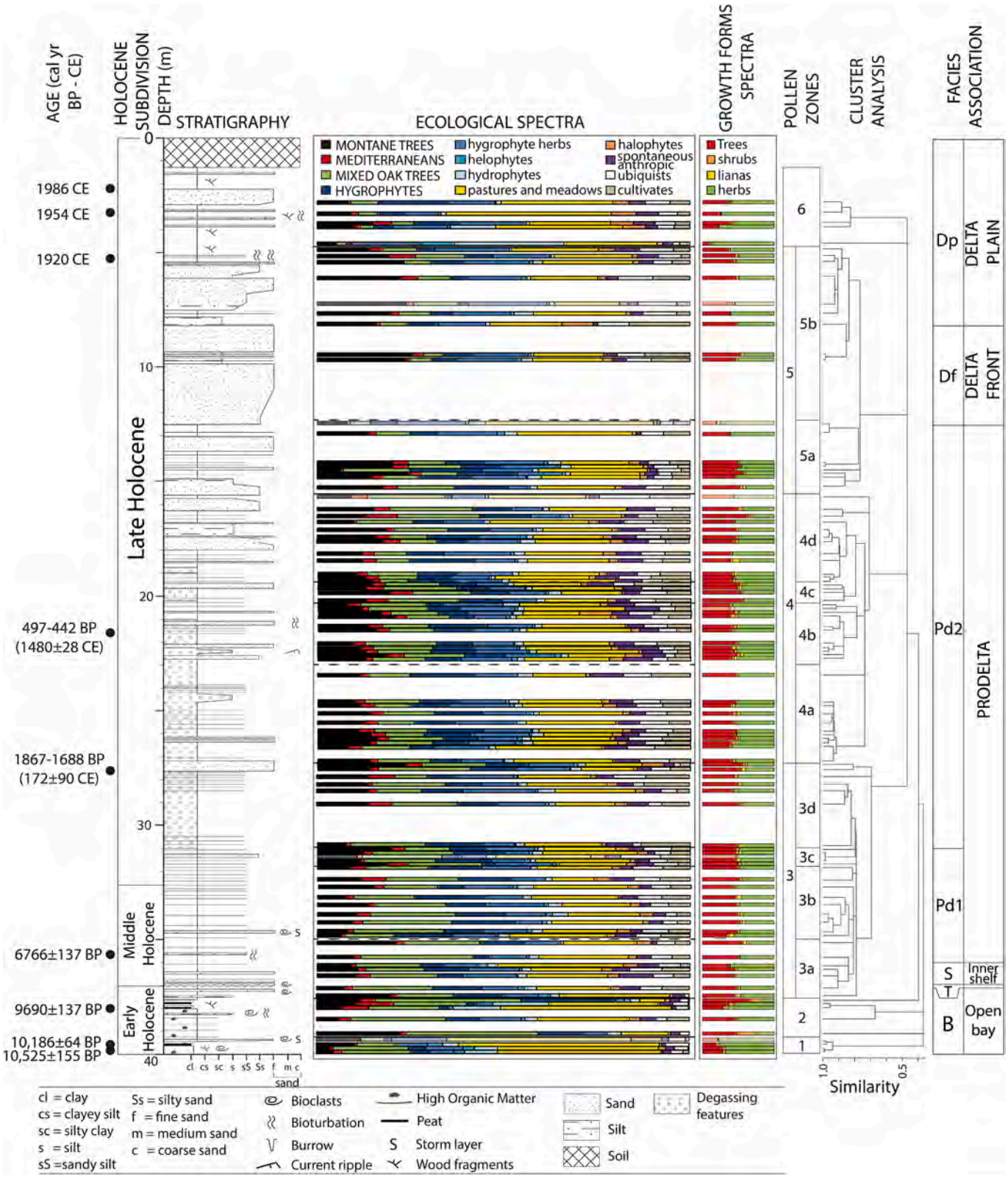

Fig. 5. Ecological and growth forms pollen spectra of core S1P, showing relative abundances of pollen groups (Table 1). Pollen zones were identified via CONISS cluster analysis and are reported on the right. Pollen data are integrated with the stratigraphic log, age markers, and facies associations. (For interpretation of the references to colour in this figure, the reader is referred to the web version of this article.)

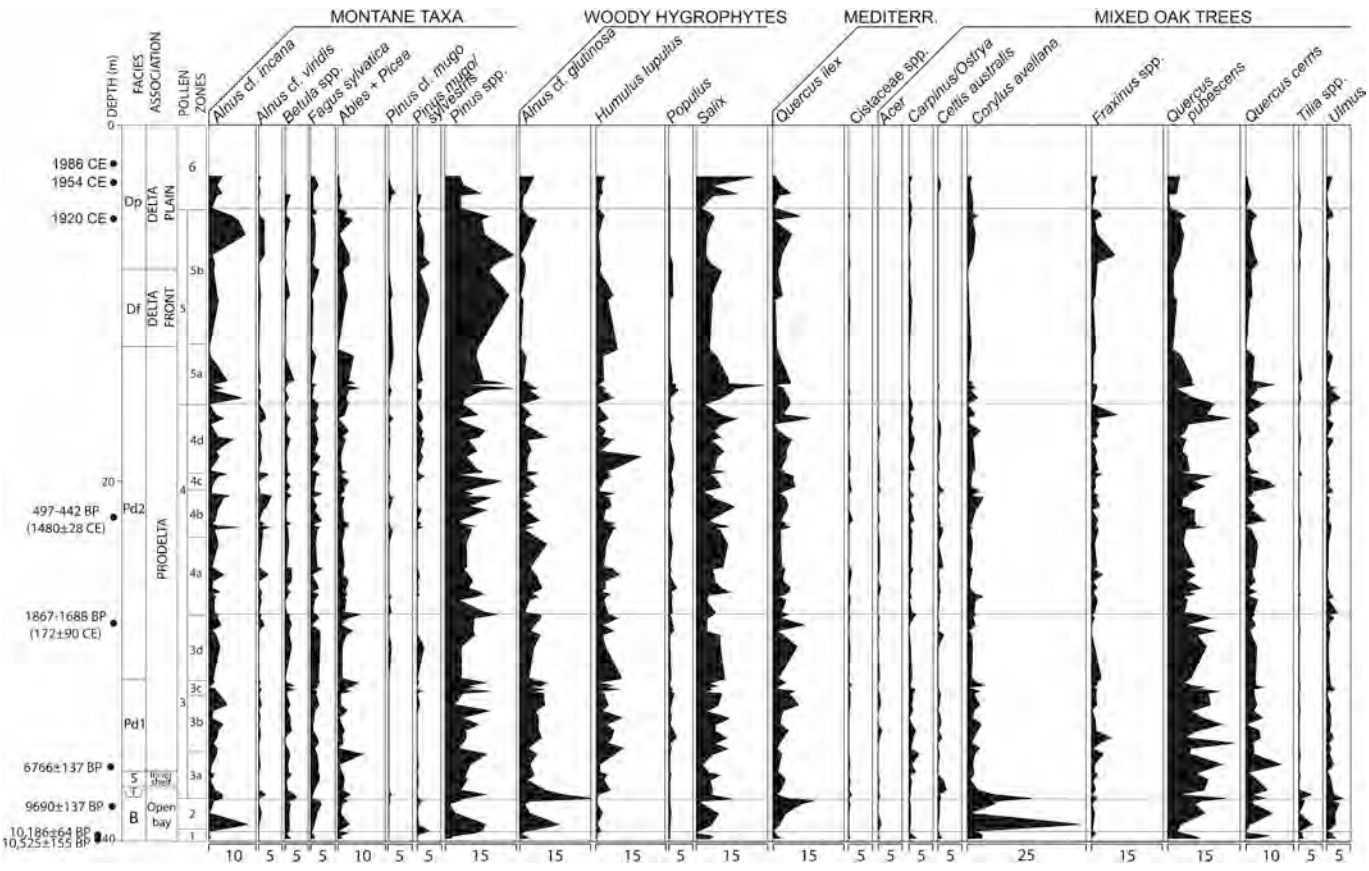

Fig. 6. Pollen percentage diagram showing the relative abundances of selected montane taxa (Mt), woody hygrophilous taxa (H), Mediterranean (M), and mixed deciduous oak taxa (Q + other deciduous trees). Chronology, facies associations, and pollen zones are reported on the left side of the diagram.

are variable, with recurrent peaks (Cc ~4–10%). The montane component is highly variable (Mt ~8–21%) and includes *Pinus* sp., *P. mugo*, *A. incana*, *Abies*, and *Fagus*. Two peaks (~21%) are recorded: the lower dominated by *A. incana* and *Fagus*; the upper by *Pinus* and *A. incana* (Fig. 6).

PZ4c (20.40–19.50 m; ~450–350 cal yr B.P.)

PZ4c comprises a thin interval of degassed muds grading upward into mud-sand alternations. Vegetation is variable, with peaks in different ecological groups and higher afforestation than in the underlying deposits (T + sh + L ~ 45–60%, Fig. 5). Meso-hygrophilus woodlands dominate, composed of deciduous oaks with *Salix*, *A. glutinosa*, abundant *Humulus*, *Ulmus*, and *Corylus* (Q ~ 8–20%). Hygrophilous trees slightly increase compared to PZ4b (H ~ 11%). The Mediterranean component is variable, but overall expanding (M ~ 3–6%). Mesophilous grasslands are extensive, dominated by spontaneous Poaceae, Cichorieae and Asteroideae (pm ~16–30%), whereas wetlands are subordinate (hyg + hel + hyd ~13%). Cultivated taxa are well represented (Cc ~6–16%), including *Castanea*, *Juglans*, and cereals; *Castanea* peaks (11%) near the top, where a marked rise in *Juglans* (>3%) is recorded (Fig. 8). Halophytes and some As taxa (e.g., *Plantago*) occasionally increase. The montane component, represented by *Pinus*, *Abies,* and *Betula* is generally moderate (Mt ~14%) but reaches a distinct peak (~20%).

PZ4d (19.50–15.60 m; ~350–225 cal yr B.P.)

PZ4d includes sand-mud alternations with a thickening-upward trend. At the base, meso-hygrophilous forests dominated by deciduous oaks (Q ~ 8–22%) are associated with *Salix*, *Alnus glutinosa* and *H. lupulus* (H ~ 18–2%), which alternate in dominance upwards. Mesophilous grasslands are widespread, dominated by spontaneous Poaceae and Chicorioideae (pm ~13–30%), while wetlands remain locally extensive (hyg + hel + hyd ~10–22%). The Mediterranean component is low and stable in the lower part, increasing upward (M ~ 2–9%). Cultivated taxa, including *Castanea*, *Juglans*, *Hordeum*-type, and later *Zea mays* (which shows its first occurrence) are consistently present (Cc ~5–10%). Indicators of disturbed environments, such as *Plantago* and Caryophyllaceae, and halophytes remain stable. The montane component, mainly *Pinus*, *Abies*, and *Alnus incana*, is constant throughout (Mt ~9–19%): montane alders and pines dominate the lower subzone, whereas upward *Pinus* prevails, *Alnus* declines, and *Abies* increases abruptly (Fig. 6). Toward the top, mixed oak woodland expands alongside rising Mediterraneans and declining mesophilous herbs.

4.4.5. PZ5 (15.60–4.90 m; ~225–25 cal yr B.P.)

PZ5 occurs in uppermost prodelta deposits and persists throughout the delta-front and the lowermost delta-plain facies association. Pollen concentrations are generally low (1.6 k/g on average), while secondary pollen percentages range 1–7%. PZ5 is subdivided into two subzones (5a and 5b).

PZ5a (15.24–12.40 m; ~225–120 cal yr B.P.)

PZ5a comprises the uppermost prodelta deposits and overlying delta-front sands. It is characterized by hygro-mesophilous vegetation dominated by forests of *Salix*, *Alnus*, *Quercus pubescens*, and *Q. cerris* (Q + H ~ 12–36%), with a generally low Mediterranean component (M < 1–4%). Mesophilous grasslands with spontaneous Poaceae, Cichorieae, and Asteroideae are extensive (pm ~20–30%). Wetlands dominated by Cyperaceae, *Carex*, and hydrophytes, such as *Hydrocharis* and *Sparganium,* are stable or expanding (hyg + hel + hyd ~8–25%, Fig. 5). Indicators of disturbed environments and halophytes fluctuate, while cultivated taxa show an overall decline. The montane component remains consistently high, except at 14.52 m, where it sharply decreases in correspondence with a marked peak in *Salix* at ~15% (Fig. 6). *Alnus incana* decreases upward as *Abies* increases, shaded by the dominance of

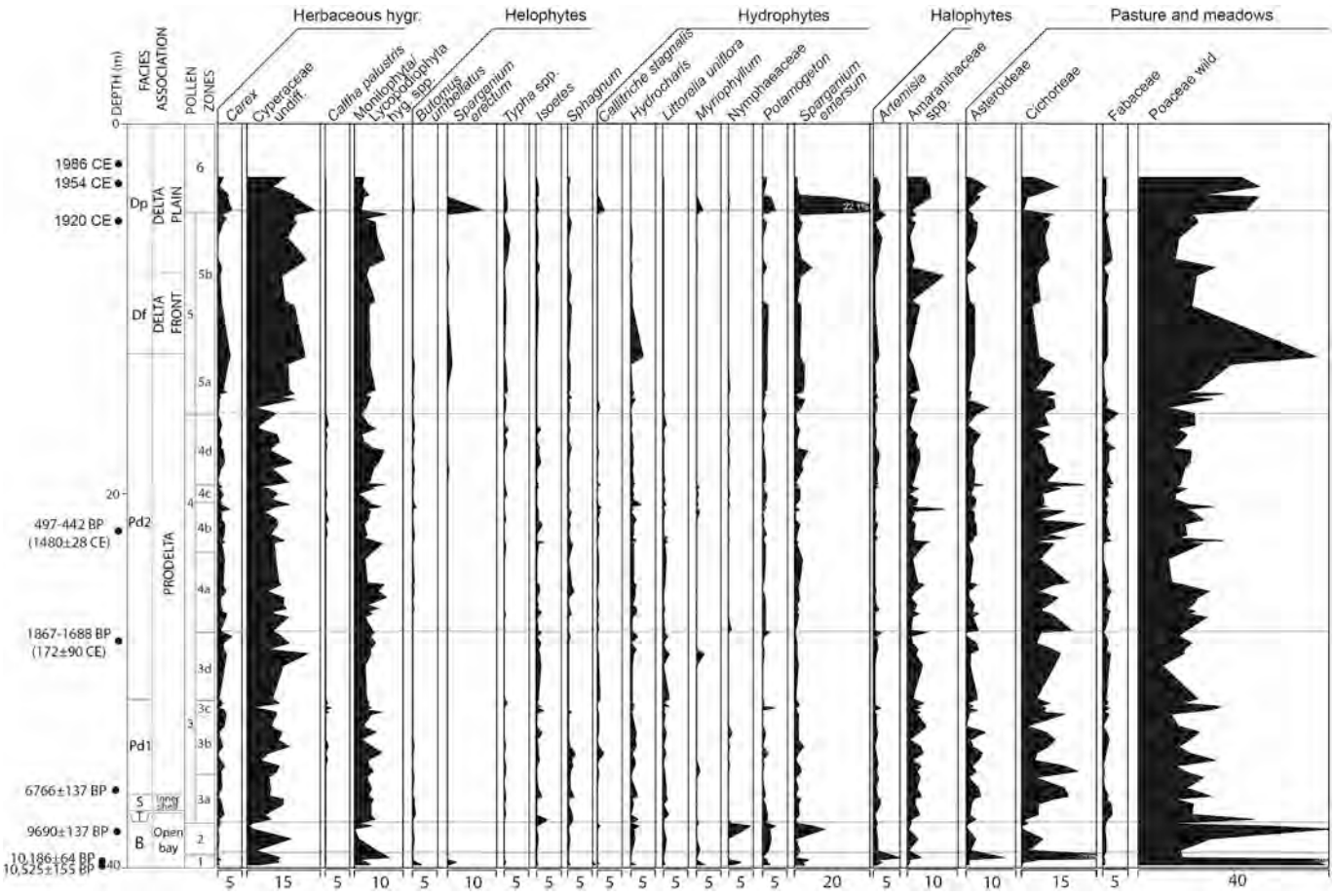

Fig. 7. Percentage pollen diagram showing herbaceous hygrophilous taxa, helophytes, hydrophytes, halophytes, and pasture-meadow taxa from core S1P. Chronology, facies associations, and pollen zones are reported on the left side of the diagram.

Pinus (Fig. 6).

PZ5b (12.40–4.90 m; ~120–25 cal yr B.P.)

PZ5b corresponds to delta-front and delta-plain deposits and it shows variable afforestation (T + sh + L ~ 40–60%, Fig. 5). The mesohygrophilous woodland is well represented, though less abundant than in underlying zones (Q + H ~ 13–21%). Mesophilous grasslands (pm ~19–26%) are consistently present with locally increasing wetlands (hyg + hel + hyd ~16–25%). The Mediterranean component, represented by *Quercus ilex*, shows a slightly increasing upward trend (M ~ 1–7%). Indicators of disturbed environments and halophytes are present, with local peaks (hal 8.5% at 8.11 m, Fig. 5). Cultivated taxa are abundant throughout (Cc 2–16%) with recurrent peaks, while ubiquists also become significant (~11%, Fig. 7). The montane component is high but fluctuating (Mt ~15–25%).

4.4.6. PZ6 (4.90-top; ~25 cal yr B.P. To present day)

This pollen zone, corresponding to recent delta-plain deposits, shows a marked shift from the underlying zones. It records the lowest afforestation of the entire sequence (T + sh + L ~ 11–43%), reflecting a clear decline in deciduous oaks (Q ~ 2–6%) and hygrophilous trees (H ~ 1.5–19%), mainly *Salix* and *Alnus* (Fig. 6). PZ6 is initially dominated by wet grasslands, with abundant *Sparganium emersum* and *S. erectum* (Fig. 7). Hygrophilous taxa, particularly *Carex* and other Cyperaceae, are also abundant. Mesophilous grasslands are represented by spontaneous Poaceae, Cichorieae and Asteroideae (pm ~22–44%). Cultivated taxa decline overall (Cc ~4%), As remains relatively stable, and halophytes slightly increase toward the top (hal ~1.5–7%). The mountain component is very low (Mt ~5–15%) and mainly represented by *Pinus*.

5. Discussion

Integrated sedimentological and palynological analyses of core S1P, supported by a robust chronological framework, highlight the strong potential of deltaic deposits to preserve records of landscape dynamics, anthropogenic activity and short-term climatic shifts. This enables comparison with regional climatic oscillations and human impacts (Fig. 9) documented across the central Mediterranean (e.g., Oldfield et al., 2003; Mercuri et al., 2012; Rasmussen et al., 2014; Magri et al., 2015; Regattieri et al., 2019).

In contrast to Early-Middle Holocene transgressive coastal to shallow-marine deposits, typically associated with depositional hiatuses and/or episodic sedimentation (Cattaneo and Steel, 2003; Bhattacharya et al., 2019, 2020), the stratigraphically expanded Late Holocene progradational deltaic succession (31 m accumulated in ~2500 years) provides a sub-centennial resolution of environmental change, locally reaching ~10 years per sample.

5.1. Early-Middle Holocene

The lowermost core interval records the Early Holocene marine ingression into the Po Plain (Amorosi et al., 2017; Bruno et al., 2017). This transgressive phase was accompanied by major vegetation shifts reflecting rapid post-glacial warming (Fig. 9A). During the Preboreal, the establishment of a partially confined open-bay environment coincided with a limited afforestation and the dominance of mesophilous grasslands (PZ1; Fig. 5), reflecting relatively cool and dry conditions within a broader warming trend (Magri et al., 2015). During the Boreal (PZ2), mixed deciduous forests markedly expanded, primarily driven by

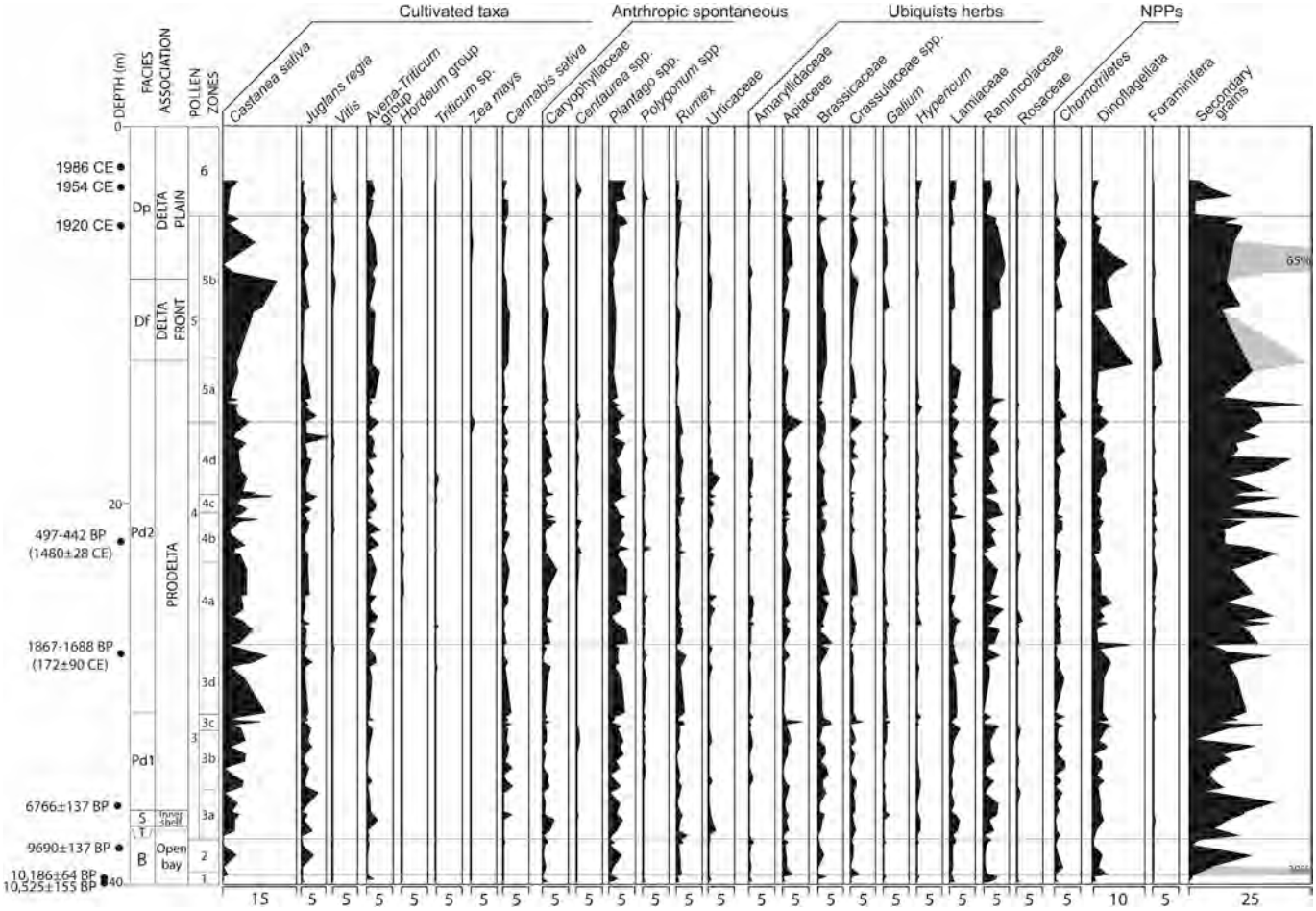

Fig. 8. Percentage pollen diagram showing cultivated, anthropic spontaneous, ubiquist taxa, non-pollen palynomorphs (NPPs), and secondary grains from core S1P. Chronology, facies associations, and pollen zones are reported on the left side of the diagram.

a sharp increase in hazel (Fig. 6; Huntley and Birks, 1983), a fast-growing, pioneer broadleaved shrub widely documented in Italian pollen records (Magri and Sadori, 1999). Significantly, at the Preboreal-Boreal transition, the concurrent rise in montane taxa (Fig. 9A), particularly pine and *A. incana* (Fig. 6), may indicate either early lowland conifer recolonization (Accorsi et al., 2004) or the short-lived cooling event associated with the 10.3 kyr B.P. climatic oscillation (Bond et al., 1997; Mayewski et al., 2004; Rasmussen et al., 2014).

The establishment of a *Quercus*-dominated mixed forest (Fig. 9A) and the first significant occurrence of Mediterranean taxa (mainly *Quercus ilex,* in Fig. 6) mark the onset of warmer and more humid conditions typical of the Holocene Climatic Optimum (HCO). This interval likely reflects a further phase of lowland recolonization and the development of Holocene coastal forests (Ferrari, 1997;Accorsi et al., 2004). Pollen assemblages indicate largely natural vegetation, as local increases in *Castanea sativa* and *Juglans regia* (together up to 7%, Fig. 8) are interpreted as following the natural reforestation. A minor peak in montane taxa (Fig. 9A) may correspond to the 9.3 kyr cold event, widely documented in European and Mediterranean records (Wanner et al., 2011; Rasmussen et al., 2014).

The transition to thin transgressive-barrier and inner-shelf deposits, together with the shift from a deepening-upward to shallowing-upward trend marked by distal prodelta (Pd1) deposits, records the maximum marine ingression and the following (early) phase of delta progradation, the latter promoted by relatively stable sea-level conditions (Vacchi et al., 2016; Amorosi et al., 2019). This interval, spanning from the early Atlantic to the Subboreal, exhibits the lowest SAR (~0.11 cm/yr) of the entire succession, indicating pronounced stratigraphic condensation under low fluvial input (Fig. 9A). Vegetation changes (PZ3a-3b) document the full development of mixed deciduous mesohygrophilous oak and alder-willow forests, reflecting persistently warm and humid conditions (Fig. 9A). This pattern is consistent with the full establishment of the HCO, marked by maximum post-glacial forest cover across Europe (Roberts et al., 2018) and local wetland expansion (Accorsi et al., 2004), and has been previously documented by other pollen-based reconstructions from the Po Plain (Cacciari et al., 2020).

5.2. Late Holocene

Although a further deceleration in relative sea-level occurred since ~4 kyr B.P. (Vacchi et al., 2016), the study area remained sediment-starved for a prolonged period, lying ~30 km offshore as late as at the Bronze Age (Correggiari et al., 2005b, Fig. 1). The pronounced peak in montane taxa between ~3.2 and ~ 2.8 kyr B.P. identified in uppermost Pd1 (PZ3c; Fig. 5) may correspond to the well-documented cooling at the Bronze-Iron Age transition (Fig. 9A), widely recognized across Europe and the Mediterranean (Bond et al., 1997; Mayewski et al., 2004; Wanner et al., 2011; Magny et al., 2013). A similar increase in montane taxa has been observed in a continental Po Plain pollen record (Cacciari et al., 2020); therefore, S1P supports the interpretation of a regional climatic signal.

5.2.1. Iron Age and the Roman Period

Enhanced sediment flux, recorded at the transition to strongly river-influenced (Pd2) prodelta deposits, started in the late Iron Age. From this time onward, high sedimentation rates markedly improved the

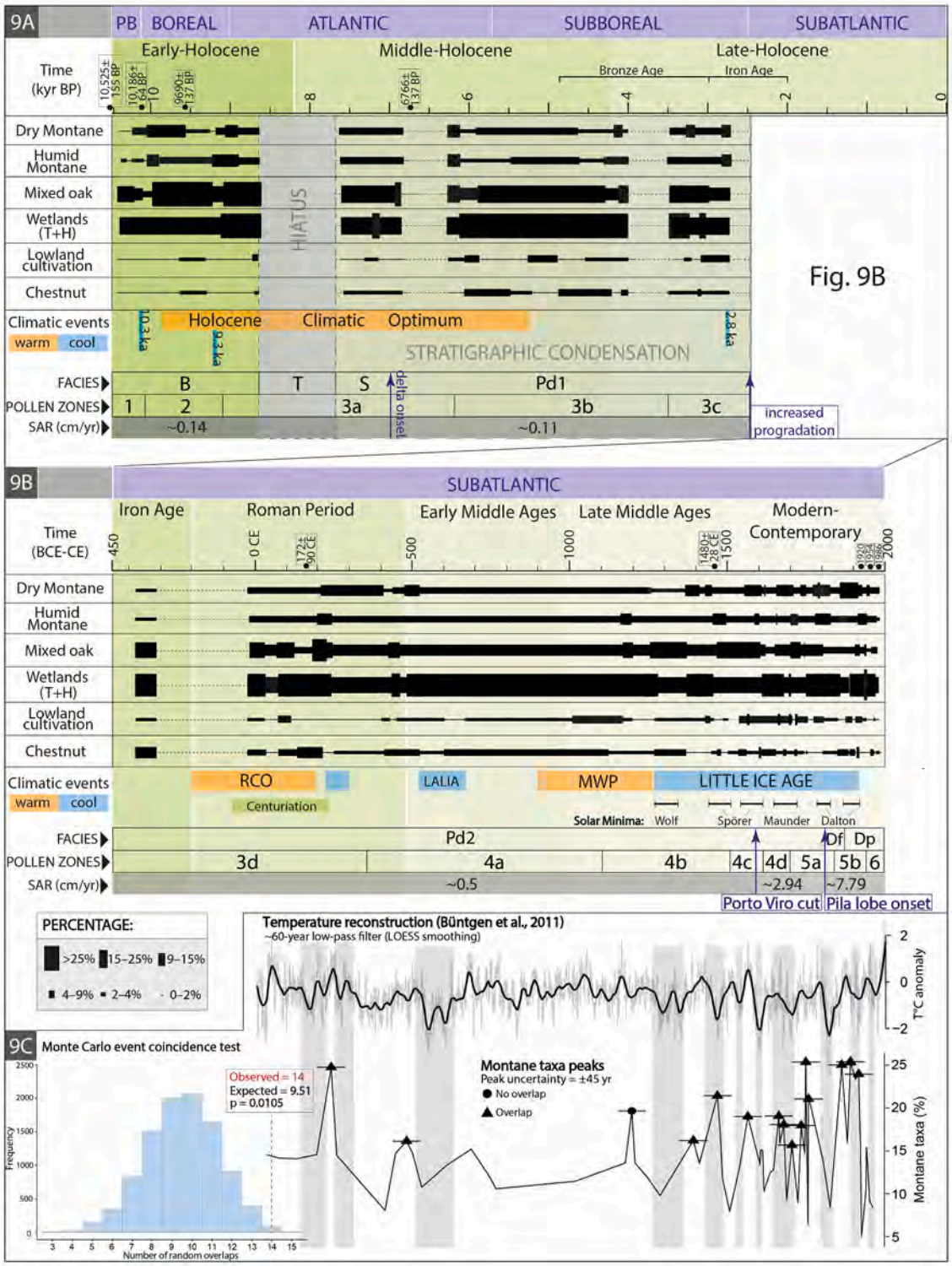

Fig. 9. Time-based synthesis of the S1P pollen record represented by selected ecological groups. The relative abundance of each group is represented through thick-lines, classified by percentages, along the time axis. Pollen data are compared with facies associations, sediment accumulation rates (SAR), climatic events, and a temperature curve for the Late Holocene (Büntgen et al., 2011). Blue arrows indicate the main phases of Po Delta development. (9 A) Holocene timeline overview, showing long-term vegetational shifts. (9B) Close-up view of the Late Holocene timeline covering the last 2500 years. (9C) Comparison between montane taxa peaks and independently defined multi-decadal cooling phases (grey bands) based on the European temperature reconstruction (Büntgen et al., 2011). Peaks in montane taxa were treated as temporal windows using a ± 45-year age uncertainty, representing an average estimate derived from the variable 95% confidence intervals of the age-depth model across the last 2000 years, and tested against cold intervals through a Monte Carlo event-coincidence approach. The histogram shows the distribution of random overlaps, while the vertical dashed line marks the observed number of coincidences. PB: Preboreal; RCO: Roman Climatic Optimum; LALIA: Late Antique Little Ice Age; MWP: Medieval Warm Period. Historical periods subdivision after Zamboni (2021). (For interpretation of the references to colour in this figure legend, the reader is referred to the web version of this article.)

temporal resolution of the core to the decadal to sub-centennial scale, enabling detection of subtle changes in vegetation, climate and human activity (Fig. 9B).

A pronounced peak in cultivated arboreal trees, mainly *Castanea sativa* (~9%; Fig. 8), at the base of PZ3d represents the first evidence of chestnut cultivation age modelled at ~2.4 kyr B.P. Pre-Roman occurrences of *Castanea sativa* have been reported at other Italian sites (Lowe et al., 1996; Mercuri et al., 2013), suggesting Iron Age cultivation (Mercuri et al., 2002; Sadori et al., 2010). However, high percentages similar to those recorded in PZ3d are generally attributed in northern Italy to the Roman period and later (Lowe et al., 1996; Oldfield et al., 2003; Conedera et al., 2004). In upper PZ3d, increased cereal pollen, particularly *Avena-Triticum* (Fig. 8), suggests extensive land reclamation and lowland cultivation during the Roman "centuriation" phase (Fig. 9B; Cremonini et al., 2013; Marchesini and Marvelli, 2017, 2018). During the Roman Climatic Optimum (RCO), a period of mild climatic conditions, montane taxa remained relatively low, with a concomitant expansion of lowland forests (wetlands and mixed oak forests, Fig. 9B). A subsequent peak in montane taxa around ~1700 yr B.P. (Roman Period), coupled with a decline in cultivated plants, may reflect the vegetation response to a brief cooling episode documented across Europe in the third century CE (Wanner et al., 2011) and the concomitant demographic decline due to the Plague of Cyprian. This followed another pandemic event around 165 CE (Zonneveld et al., 2024) and the interval also coincides with a period of political and social instability in the Roman Empire, which resulted in partial abandonment of centuriated lands (Cremonini et al., 2013).

5.2.2. The Middle Ages / Modern Age

Within the prograding Pd2 succession, pollen zone PZ4a captures the onset of the Late Antique Little Ice Age (LALIA, ~1410–1290 cal yr B.P.; ~536–660 CE), a widespread cooling phase across the Northern Hemisphere likely triggered by intense volcanic eruptions (Büntgen et al., 2016). The effects of this climatic deterioration are evident in the basal PZ4a, where an increase in montane taxa is followed by a marked decline in cultivated species (Fig. 9B). This pattern likely reflects the combined effect of climatic cooling and societal crises associated with the Justinian plague (~540 CE; Zonneveld et al., 2024) and the Ostrogothic-Byzantine wars (535–553 CE), which led to widespread settlement collapse (Ostrogorski, 1968) and contraction of crop fields. Cultivated taxa then increase again until ~1000 yr B.P., reflecting renewed agricultural expansion following Early Medieval land reclamation (Fig. 9B). A vegetation pattern similar to RCO is recorded during the Medieval Warm Period (MWP), characterized by well developed lowland forests and relatively low montane taxa, with an additional expansion of lowland cultivation.

Uppermost Pd2 deposits record increased climatic variability associated with the onset of the Little Ice Age (LIA), a prolonged cooling phase linked to reduced solar irradiance between the mid-13th and late 19th centuries CE that left a strong stratigraphic expression (e.g. Cattaneo et al., 2003; Pellegrini et al., 2021). The LIA encompasses four major Solar Minima (Wanner et al., 2022): Wolf (~1280–1350 CE), Spörer (~1460–1550 CE), Maunder (~1645–1715 CE), and Dalton (~1790–1830 CE). Vegetation patterns (PZ4b-PZ5) show pronounced oscillations among ecological groups: peaks in montane taxa chronologically align with Solar Minima (Spörer, Maunder and Dalton; Fig. 9B) and generally correspond to declines in cultivated species. Given the strong reliance of pre-industrial societies on agriculture, this recurrent pattern suggests a link between colder climatic phases and periods of socio-economic stress.

Variable vegetation responses suggest differing moisture regimes associated with the distinct LIA cooling phases. Since pollen assemblages were deposited in a prodelta setting, the local origin of montane taxa can be excluded, as these taxa do not naturally grow in lowland coastal environments during the investigated intervals; their occurrence is therefore interpreted as primarily reflecting a regional signal. The peak in montane taxa in upper PZ4b, ascribed to the Spörer Minimum, is characterized by pine dominance with subordinate alder, indicating cool and dry conditions (Wanner et al., 2022). The Maunder Minimum (PZ4d), which represents the coldest phase of the LIA (Luterbacher et al., 2001; Magny et al., 2010; Büntgen et al., 2011), was characterized by the predominance of conifers (*Pinus* spp. and *Abies alba*, Fig. 6).

Two pronounced peaks in montane taxa observed in PZ5a and PZ5b, respectively (Fig. 5), are interpreted as vegetation responses to the Dalton Minimum (1790–1830 CE, Steinhilber et al., 2009). In the lower interval, the co-occurrence of *Alnus incana* and *Pinus* (Fig. 6) suggests relatively cool and humid conditions. Upsection, the replacement of humid montane by dry montane taxa indicates a transition toward cooler and drier conditions (Fig. 9B). The overall increase in montane taxa (mainly *Pinus* sp., Fig. 6) within PZ5b may partially originate from the extensive coastal pine plantations emplaced during this period, the remnants of which persist today (Piccoli et al., 1983). From the second half of the 19th century human intervention on the coastal landscape obscured the climatic signal of the later Dalton Minimum, possibly revealed by a minor *Abies alba* increase paralleled by *Pinus* sp. Overall, the S1P record confirms the sensitivity of Po river catchment vegetation to both LALIA and LIA climatic oscillations, refining the observation previously documented in the adjacent delta lobe of *Po di Goro* (Cacciari et al., 2024). In particular, the stratigraphically expanded upper portion of the S1P succession provides a higher chronological resolution of LIA-related cooling phases.

The comparison between montane taxa peaks and independently defined cold intervals reveals a non-random temporal coincidence between vegetation dynamics and climate variability over the last two millennia. A substantial proportion of montane peaks (>90%) fall within or overlap multi-decadal periods of sustained negative temperature anomalies identified from the smoothed reconstruction of Büntgen et al. (2011) (Fig. 9C). The Monte Carlo test shows that the observed number of overlaps exceeds the expected random distribution (expected = 9.51, observed = 14, $p = 0.0105$, Fig. 9C).

These results suggest that phases of enhanced montane taxa expansion tend to occur preferentially during cooler climatic conditions. The agreement between the independently defined cold phases and well-known historical climatic deteriorations (e.g., LALIA, Solar Minima) further supports the climatic significance of the detected signal.

However, the relationship is not strictly deterministic, as not all cold intervals from Büntgen et al. (2011) are associated with pronounced montane peaks, and some variability remains unexplained. This indicates that additional factors such as record resolution, sedimentary dynamics and/or anthropogenic impact, likely influence the expression and preservation of the montane signal in the sedimentary record.

The most intense phase of delta progradation, recorded in the uppermost 20 m was driven in large part by human activities. Among these: (i) the *Porto Viro* diversion (1600–1604), which redirected Po River sediment southward, promoting rapid progradation of a new delta lobe and contributing to the development of the modern cuspate delta morphology (Maselli and Trincardi, 2013); (ii) the artificial W-E straightening of the main feeding river trunk (1886 CE), which led to the dominance of the modern *Po di Pila* branch (Correggiari et al., 2005b).

Interestingly, following the Porto Viro diversion, the pollen record shows more frequent peaks in secondary pollen (Fig. 8), likely indicative of enhanced fluvial input and/or erosion in the catchment associated with this major hydraulic intervention.

From the base of PZ5a onward (~1745 CE), cereals show a marked increase and maintain consistently higher percentages than in older intervals, indicating a more sustained phase of agricultural intensification. A similar trend is observed for other cultivated species, such as *Cannabis sativa* and *Juglans regia*. The first occurrence of *Zea mays* at the base of PZ5a provides an additional chronological marker, confirming modelled ages more recent than the end of the XVI century (Cazzola, 1988). In the topmost portion of the record, facies-driven signals dominate over regional patterns. In PZ6, the abrupt decline in

afforestation and the increase in aquatic taxa (notably *Sparganium*, Fig. 7) document wetland development (Fig. 9B). The subsequent increase in halophytic taxa (Fig. 5; e.g. Amaranthaceae) reflects vegetation typical of coastal dunes and brackish habitats of the modern delta plain.

6. Conclusions

Deltaic successions can provide robust archives for reconstructing Holocene environmental change. In the Po Delta, the relative contribution of river dynamics, climate variability, and anthropogenic forcing is clearly reflected by the pollen signal of core S1P. The integration of radiocarbon dating (7 AMS ^{14}C samples), short-lived radionuclide (^{210}Pb and ^{137}Cs) analyses, and pollen-based markers (e.g. increased *Castanea sativa* and cereals, first occurrence of *Zea mays*) provides a robust chronological framework for the study succession. The main outcomes of this study can be summarized as follows:

- Detailed facies analysis of core S1P records a Holocene transgressive-regressive trend, characterized by rapid landward shoreline migration and the establishment of inner-shelf conditions at maximum transgression (Early-Middle Holocene), followed by extensive delta progradation, particularly during the Late Holocene.
- Early Holocene pollen assemblages document the post-glacial reorganization of the Po Plain landscape from open mesophilous grasslands to mixed deciduous forests. With the onset of the Holocene Climatic Optimum, meso-hygrophilous woodlands developed, reflecting climatic amelioration, and persisted throughout the Middle Holocene. The vegetation was punctuated by short-lived increases in montane taxa, likely reflecting centennial-scale cooling events.
- The stratigraphically expanded interval spanning the last ~2500 years provides a well-resolved record of landscape-climate-human interactions. From the Iron Age onward, anthropogenic impact intensified, as reflected by peaks in cultivated taxa (cereals and chestnut). Between the 2nd-7th centuries CE, landscape changes were driven by climatic instability, pandemic events and socio-economic turmoil.
- During the LIA recurrent peaks in montane taxa are chronologically consistent with solar minima, indicating the vegetation response to centennial-scale climatic forcing even within an increasingly human-modified landscape.
- Overall, the S1P record demonstrates that, despite their complexity, deltaic successions can provide high-resolution archives of environmental change, acting as integrative systems that reflect climatic forcing, landscape dynamics, and human activity along the land-sea continuum.

Supplementary data to this article can be found online at https://doi.org/10.1016/j.palaeo.2026.113992.

Open research

The data analyzed in this study are publicly available on Zenodo at DOI: https://doi.org/10.5281/zenodo.19252028

CRediT authorship contribution statement

S. Catena: Writing – original draft, Visualization, Methodology, Investigation, Formal analysis, Data curation, Conceptualization. **V. Rossi:** Writing – review & editing, Investigation, Conceptualization. **M. Cacciari:** Writing – review & editing, Methodology, Investigation, Formal analysis. **A. Vecchi:** Writing – review & editing, Methodology, Investigation, Formal analysis, Data curation. **M. Marchesini:** Writing – review & editing, Investigation. **S. Marvelli:** Writing – review & editing, Investigation. **S. Giuliani:** Writing – review & editing, Methodology, Data curation. **L. Bellucci:** Writing – review & editing, Methodology, Data curation. **C. Pellegrini:** Writing – review & editing, Supervision, Investigation, Funding acquisition, Conceptualization. **A. Amorosi:** Writing – review & editing, Supervision, Project administration, Investigation, Funding acquisition, Conceptualization.

Funding

This study was supported by the PRIN project 2022PMEN2K "Refining the sequence stratigraphic model through high-resolution onshore-offshore correlation (ON/OFF): The late Quaternary succession of the Po-Adriatic system" founded by the Ministero dell'Università e della Ricerca, Italy.

Declaration of competing interest

The authors declare that they have no known competing financial interests or personal relationships that could have appeared to influence the work reported in this paper.

Acknowledgements

The authors would like to thank the team of palynologists and archaeobotanists of the *Centro Agricoltura e Ambiente "G. Nicoli"* (Italy) for their collaboration and support in palynological preparation procedures and analyses. The authors are grateful to Dr. Albino Irene (University of Bologna, BiGeA Department) for the preparation of micropalaeontological samples. We also thank Andrea Gallerani for assistance during laboratory sampling procedures and for core S1P photography. Special thanks are extended to Irene Sammartino and Bruno Campo for their support during sampling activities in the laboratory. We sincerely thank the Editor and the Reviewers for their constructive comments and careful evaluation of the manuscript. Their insightful suggestions substantially improved the quality, clarity, and overall robustness of the study.

Data availability

The authors confirm that all data necessary for supporting the scientific findings of this paper have been provided.

References

Accorsi, C.A., Bandini Mazzanti, M., Forlani, L., Mercuri, A.M., Trevisan, G., 2004. Holocene forest vegetation (pollen) of the Emilia–Romagna plain (Northeastern Italy). In: Bittmann, F. (Ed.), La végétation postglaciaire du passé et du présent: syngenèse, synécologie et synsystématique. J. Cramer in der Gebrüder Borntraeger Verlagsbuchhandlung, Stuttgart, pp. 1–103.

Allen, H.D., 2003. Response of past and present Mediterranean ecosystems to environmental change. Prog. Phys. Geogr. 27, 359–377. https://doi.org/10.1191/0309133303767888482.

Amorosi, A., Dinelli, E., Rossi, V., Vaiani, S.C., Sacchetto, M., 2008. Late Quaternary palaeoenvironmental evolution of the Adriatic coastal plain and the onset of Po River Delta. Palaeogeogr. Palaeoclimatol. Palaeoecol. 268, 80–90. https://doi.org/10.1016/j.palaeo.2008.07.009.

Amorosi, A., Bruno, L., Campo, B., Morelli, A., Rossi, V., Scarponi, D., Hong, W., Bohacs, K.M., Drexler, T.M., 2017. Global sea-level control on local parasequence architecture from the Holocene record of the Po Plain, Italy. Mar. Pet. Geol. 87, 99–111. https://doi.org/10.1016/j.marpetgeo.2017.01.020.

Amorosi, A., Barbieri, G., Bruno, L., Campo, B., Drexler, T.M., Hong, W., Rossi, V., Sammartino, I., Scarponi, D., Vaiani, S.C., Bohacs, K.M., 2019. Three-fold nature of coastal progradation during the Holocene eustatic highstand, Po Plain, Italy: close correspondence of stratal character with distribution patterns. Sedimentology 66, 3029–3052. https://doi.org/10.1111/sed.12621.

Amorosi, A., Bruno, L., Campo, B., Costagli, B., Dinelli, E., Hong, W., Rossi, V., Sammartino, I., Scarponi, D., Vaiani, S.C., 2020. Tracing clinothem geometry and sediment pathways in the prograding Holocene Po Delta system through integrated core stratigraphy. Basin Res. 32, 206–215.

Andersen, S.T., 1979. Identification of wild grass and cereal pollen. Danmarks Geol. Unders. Årbog 1978, 69–92.

Anthony, E.J., Marriner, N., Morhange, C., 2014. Human influence and the changing geomorphology of Mediterranean deltas and coasts over the last 6000 years: from

progradation to destruction phase? Earth Sci. Rev. 139, 336–361. https://doi.org/10.1016/j.earscirev.2014.10.003.
Appleby, P.G., 1998. Dating recent sediments by ˆ210Pb: Problems and solutions. In: Ilus, E. (Ed.), Use of 210Pb and 137Cs in Sediment Dating. STUK, Helsinki, pp. 7–24. STUK-A 145.
Artegiani, A., Paschini, E., Russo, A., Bregant, D., Raicich, F., Pinardi, N., 1997. The Adriatic Sea general circulation. Part II: baroclinic circulation structure. J. Phys. Oceanogr. 27, 1515–1532. https://doi.org/10.1175/1520-0485(1997)027<1515:TASGCP>2.0.CO;2.
Athersuch, J., Horne, D.J., Whittaker, J.E., 1989. Marine and Brackish Water Ostracods (Superfamilies Cypridacea and Cytheracea): Keys and Notes for the Identification of the Species. E.J. Brill, Leiden.
Barbieri, G., Rossi, V., Vaiani, S.C., Horton, B.P., 2019. Benthic ostracoda and foraminifera from the North Adriatic Sea (Italy, Mediterranean Sea): a proxy for the depositional characterisation of river-influenced shelves. Mar. Micropaleontol. 153, 101772. https://doi.org/10.1016/j.marmicro.2019.101772.
Barbieri, G., Rossi, V., Vaiani, S.C., Dasgupta, U., Amorosi, A., 2021. Quantitative paleoecology in shallow-marine settings: the value of ostracods and foraminifers from the Holocene North Adriatic record. Palaeogeogr. Palaeoclimatol. Palaeoecol. 572, 110408. https://doi.org/10.1016/j.palaeo.2021.110408.
Bassetti, M.A., Berné, S., Sicre, M.A., Dennielou, B., Alonso, Y., Buscail, R., Jalali, B., Heussner, S., Kerhervé, P., Menniti, C., 2016. Holocene hydrological changes in the Rhône River (NW Mediterranean) as recorded in the marine mud belt. Climate Past 12, 1539–1553. https://doi.org/10.5194/cp-12-1539-2016.
Beaudouin, C., Suc, J.P., Cambon, G., Touzani, A., Giresse, P., Pont, D., Aloïsi, J.C., Ferrier, J., 2005. Present-day rhythmic deposition in the Grand Rhône prodelta (NW Mediterranean) according to high-resolution pollen analyses. J. Coast. Res. 21, 292–306. https://doi.org/10.2112/02-878.1.
Bellucci, L.G., Frignani, M., Cochran, J.K., Albertazzi, S., Zaggia, L., Cecconi, G., Hopkins, H., 2007. 210Pb and 137Cs as chronometers for salt marsh accretion in the Venice Lagoon: links to flooding frequency and climate change. J. Environ. Radioact. 97, 85–102. https://doi.org/10.1016/j.jenvrad.2007.03.005.
Berger, J., Lespez, L., Kuzucuoğlu, C., Glais, A., Hourani, F., Barra, A., Guilaine, J., 2016. Interactions between climate change and human activities during the early tomid-Holocene in the eastern Mediterranean basins. Clim. Past 12, 1847–1877. https://doi.org/10.5194/CP-12-1847-2016.
Berglund, B.E., Ralska-Jasiewiczowa, M., 1986. Pollen analysis and pollen diagrams. In: Berglund, B.E. (Ed.), Handbook of Holocene Palaeoecology and Palaeohydrology. John Wiley & Sons, Chichester, pp. 455–484.
Bernhardt, C.E., Horton, B.P., Stanley, J.D., 2012. Nile Delta vegetation response to Holocene climate variability. Geo. 40, 615–618. https://doi.org/10.1130/G33012.1.
Besset, M., Anthony, E.J., Bouchette, F., 2019. Multi-decadal variations in delta shorelines and their relationship to river sediment supply: an assessment and review. Earth Sci. Rev. 193, 199–219. https://doi.org/10.1016/j.earscirev.2019.04.018.
Bever, A.J., Harris, C.K., Sherwood, C.R., Signell, R.P., 2009. Deposition and flux of sediment from the Po River, Italy: an idealized and wintertime numerical modeling study. Mar. Geol. 260, 69–80. https://doi.org/10.1016/j.margeo.2009.01.007.
Bhattacharya, J.P., Miall, A.D., Ferron, C., Gabriel, J., Randazzo, N., Kynaston, D., Jicha, B.R., Singer, B.S., 2019. Time-stratigraphy in point sourced river deltas: application to sediment budgets, shelf construction, and paleo-storm records. Earth Sci. Rev. 199, 102985. https://doi.org/10.1016/j.earscirev.2019.102985.
Bhattacharya, J.P., Howell, C.D., MacEachern, J.A., Walsh, J.P., 2020. Bioturbation, sedimentation rates, and preservation of flood events in deltas. Palaeogeogr. Palaeoclimatol. Palaeoecol. 560, 110049. https://doi.org/10.1016/j.palaeo.2020.110049.
Birks, H.H., Birks, H.J.B., 2006. Multi-proxy studies in palaeolimnology. Veget. Hist. Archaeobot. 15, 235–251. https://doi.org/10.1007/s00334-006-0066-6.
Blaauw, M., Christen, J.A., 2011. Flexible paleoclimate age-depth models using an autoregressive gamma process. Bayesian Anal. 6, 457–474. https://doi.org/10.1214/11-BA618.
Blackmore, S., Steinmann, J.A., Hoen, P.P., Punt, W., 2003. Betulaceae and Corylaceae. Rev. Palaeobot. Palynol. 123, 71–98.
Blasi, C., Michetti, L., 2007. The climate of Italy. In: Blasi, C., Boitani, L., La Posta, S., Manes, F., Marchetti, M. (Eds.), Biodiversity in Italy. Palombi Editori, Rome, pp. 57–66.
Blasi, C., Capotorti, G., Copiz, R., Guida, D., Mollo, B., Smiraglia, D., Zavattero, L., 2014. Classification and mapping of the ecoregions of Italy. Plant Biosyst. 148, 1255–1345. https://doi.org/10.1080/11263507909426417.
Bonaduce, G., Ciampo, G., Masoli, M., 1975. Distribution of Ostracoda in the Adriatic Sea. Pubblicazioni della Stazione Zool. Napoli 40, 1–154.
Bond, G., Showers, W., Cheseby, M., Lotti, R., Almasi, P., DeMenocal, P., Priore, P., Cullen, H., Hajdas, I., Bonani, G., 1997. A pervasive millennial-scale cycle in North Atlantic Holocene and glacial climates. Science 278, 1257–1266. https://doi.org/10.1126/science.278.5341.1257.
Bondesan, M., Favero, V., Viñals, M.J., 1995. New evidence on the evolution of the Po-delta coastal plain during the Holocene. Quat. Int. 29-30, 105–110. https://doi.org/10.1016/1040-6182(95)00012-8.
Breman, E., 1975. The Distribution of Ostracodes in the Bottom Sediments of the Adriatic Sea. Free University of Amsterdam, The Netherlands. PhD Thesis.
Brown, A.G., Carpenter, R.G., Walling, D.E., 2007. Monitoring fluvial pollen transport, its relationship to catchment vegetation and implications for palaeoenvironmental studies. Rev. Palaeobot. Palynol. 147, 60–76. https://doi.org/10.1016/j.revpalbo.2007.06.005.
Bruno, L., Bohacs, K.M., Campo, B., Drexler, T.M., Rossi, V., Sammartino, I., Scarponi, D., Hong, W., Amorosi, A., 2017. Early Holocene transgressive palaeogeography in the Po coastal plain (northern Italy). Sedimentology 64, 1792–1816. https://doi.org/10.1111/sed.12374.
Büntgen, U., Tegel, W., Nicolussi, K., McCormick, M., Frank, D., Trouet, V., Kaplan, J.O., Herzig, F., Heussner, K.-U., Wanner, H., Luterbacher, J., Esper, J., 2011. 2500 years of European climate variability and human susceptibility. Science 331, 578–582. https://doi.org/10.1126/science.1197175.
Büntgen, U., Myglan, V.S., Ljungqvist, F.C., McCormick, M., Di Cosmo, N., Sigl, M., Jungclaus, J., Wagner, S., Krusic, P.J., Esper, J., Kaplan, J.O., De Vaan, M.A.C., Luterbacher, J., Wacker, L., Tegel, W., Kirdyanov, A.V., 2016. Cooling and societal change during the late Antique Little Ice Age from 536 to around 660 AD. Nat. Geosci. 9, 231–236. https://doi.org/10.1038/ngeo2652.
Cacciari, M., Amorosi, A., Marchesini, M., Kaniewski, D., Bruno, L., Campo, B., Rossi, V., 2020. Linking Holocene vegetation dynamics, palaeoclimate variability and depositional patterns in coastal successions: insights from the Po Delta plain of northern Italy. Palaeogeogr. Palaeoclimatol. Palaeoecol. 538, 109468. https://doi.org/10.1016/j.palaeo.2019.109468.
Cacciari, M., Amorosi, A., Marchesini, M., Marvelli, S., Rossi, V., 2024. From the Roman Empire to the present: two millennia of pollen-based environmental changes and climate–human interactions in the Po Delta area (NE Italy). The Holocene 34, 1225–1241. https://doi.org/10.1177/09596836241254487.
Catena, S., Marchesini, M., Marvelli, S., Amorosi, A., 2026. Pollen Counts Dataset from Core S1P (Po Delta, northeastern Italy). https://doi.org/10.5281/zenodo.19252028.
Cattaneo, A., Steel, R.J., 2003. Transgressive deposits: a review of their variability. Earth Sci. Rev. 62, 187–228.
Cattaneo, A., Correggiari, A., Langone, L., Trincardi, F., 2003. The late-Holocene Gargano subaqueous delta, Adriatic shelf: sediment pathways and supply fluctuations. Mar. Geol. 193, 61–91.
Cazzola, F., 1988. L'introduzione del mais in Italia e la sua utilizzazione alimentare (sec. XVI-XVIII). In: La preparation alimentaire des céréales. Rapports presentes a la Table ronde.
Chelli, S., Wellstein, C., Campetella, G., Canullo, R., Tonin, R., Zerbe, S., Gerdol, R., 2017. Climate change response of vegetation across climatic zones in Italy. Climate Res 71, 249–262. https://doi.org/10.3354/cr01443.
Conedera, M., Krebs, P., Tinner, W., Pradella, M., Torriani, D., 2004. The cultivation of *Castanea sativa* (Mill.) in Europe, from its origin to its diffusion on a continental scale. Veg. Hist. Archaeobotany 13, 161–179. https://doi.org/10.1007/s00334-004-0038-7.
Correggiari, A., Cattaneo, A., Trincardi, F., 2005a. The modern Po Delta system: Lobe switching and asymmetric prodelta growth. Mar. Geol. 222-223, 49–74. https://doi.org/10.1016/j.margeo.2005.06.039.
Correggiari, A., Cattaneo, A., Trincardi, F., 2005b. Depositional patterns in the late Holocene Po delta system. In: Giosan, L., Bhattacharya, J.P. (Eds.), River Deltas—Concepts, Models, and Examples, 83. SEPM (Society for Sedimentary Geology) Special Publication, Tulsa, pp. 365–392. https://doi.org/10.2110/pec.05.83.0365.
Cremaschi, M., Bernabo Brea, M., Tirabassi, J., et al., 1980. L'evoluzione della pianura emiliana durante l'Eta del Bronzo, l'Eta Romana e l'Alto Medio Evo: Geomorfologia ed insediamenti. Padusa 16, 1–106.
Cremonini, S., Labate, D., Curina, R., 2013. The late-antiquity environmental crisis in Emilia region (Po river plain, Northern Italy): geoarchaeological evidence and paleoclimatic considerations. Quat. Int. 316, 162–178. https://doi.org/10.1016/j.quaint.2013.09.014 d'Italia. Min. Agr. Foreste, Collana verde 27, Roma.
Di Rita, F., Celant, A., Milli, S., Magri, D., 2015. Lateglacial-early Holocene vegetation history of the Tiber delta (Rome, Italy) under the influence of climate change and sea level rise. Rev. Palaeobot. Palynol. 218, 204–216. https://doi.org/10.1016/j.revpalbo.2014.12.005.
Di Rita, F., Ghilardi, M., Aranbarri, J., Fagel, N., Vacchi, M., Warichet, F., Delanghe, D., Sicurani, J., Martinet, L., Robresco, S., 2022. Natural and anthropogenic dynamics of the coastal environment in northwestern Corsica (western Mediterranean) over the past six millennia. Quat. Sci. Rev. 278, 107372. https://doi.org/10.1016/j.quascirev.2022.107372.
Dusar, B., Verstraeten, G., Notebaert, B., Bakker, J., 2011. Holocene environmental change and its impact on sediment dynamics in the Eastern Mediterranean. Earth Sci. Rev. 108, 137–157. https://doi.org/10.1016/j.earscirev.2011.06.006.
Ellis, B.F., Messina, A.R., 1940. Catalogue of Foraminifera. Cushman Laboratory for Foraminiferal Research, Sharon, MA.
Ellis, B.F., Messina, A.R., 1952. Catalogue of Ostracoda. American Museum of Natural History, New York.
Fanget, A.S., Bassetti, M.A., Fontanier, C., Tudryn, A., Berné, S., 2016. Sedimentary archives of climate and sea-level changes during the Holocene in the Rhône prodelta (NW Mediterranean Sea). Climate Past 12, 2161–2179. https://doi.org/10.5194/cp-12-2161-2016.
Ferrari, C, 1997. The vegetation belts of Emilia-Romagna (Northern Italy). Allionia 34, 219–231.
Florenzano, A., Mercuri, A.M., Pederzoli, A., Torri, P., Bosi, G., Olmi, L., Rinaldi, R., Bandini Mazzanti, M., 2012. The significance of intestinal parasite remains in pollen samples from medieval pits in Piazza Garibaldi of Parma, Emilia-Romagna, northern Italy. Geoarch 27, 34–47. https://doi.org/10.1002/gea.21390. Object Identifier (DOI).
Frignani, M., Sorgente, D., Langone, L., Albertazzi, S., Ravaioli, M., 2004. Behavior of Chernobyl radiocesium in sediments of the Adriatic Sea off the Po River delta and the Emilia-Romagna coast. J. Environ. Radioact. 71, 299–312. https://doi.org/10.1016/S0265-931X(03)00175-9.
Galloway, W.E., 1975. Process Framework for Describing the Morphologic and Stratigraphic Evolution of Deltaic Depositional Systems 87–98.

Gamberi, F., Pellegrini, C., Dalla Valle, G., Scarponi, D., Bohacs, K.M., Trincardi, F., 2020. Compound and hybrid clinothems of the last lowstand Mid-Adriatic Deep: processes, depositional environments, controls and implications for stratigraphic analysis of prograding systems. Basin Res. 32, 363–377. https://doi.org/10.1111/bre.12417.

García-García, A., Orange, D.L., Miserocchi, S., Correggiari, A., Langone, L., Lorenson, T. D., Trincardi, F., Nittrouer, C.A., 2007. What controls the distribution of shallow gas in the Western Adriatic Sea? Cont. Shelf Res. 27, 359–374. https://doi.org/10.1016/j.csr.2006.11.003.

Ghilardi, M., Revelles, J., Mary, J.-B., Di Rita, F., Delhon, C., Delangh, D., Robresco, S., 2023. Mid- to Late-Holocene coastal morphological evolution, vegetation history and land-use changes of the Porto Gulf UNESCO World Heritage site and its surroundings (NW Corsica Island, Western Mediterranean). The Holocene 33, 1023–1044. https://doi.org/10.1177/09596836231176492.

Ghilardi, M., Revelles, J., Vacchi, M., Pasquet, A., Brkojewitsch, G., 2026. Reconstructing landscape configuration, vegetation history and land-use in the coastal area of two Western Mediterranean Islands (Corsica and Cavallo Islands): evidence for a Roman environmental tipping point. Palaeogeogr. Palaeoclimatol. Palaeoecol. 113608. https://doi.org/10.1016/j.palaeo.2026.113608.

Gibling, M.R., 2018. River systems and the anthropocene: a late pleistocene and holocene timeline for human influence. Quaternary 1, 21. https://doi.org/10.3390/quat1030021.

Grimm, E.C., 1987. CONISS: a FORTRAN 77 program for stratigraphically constrained cluster analysis by the method of incremental sum of squares. Comput. Geosci. 13, 13–35. https://doi.org/10.1016/0098-3004(87)90022-7.

Hammer, Ø., Harper, D.A.T., Ryan, P.D., 2001. PAST: Paleontological statistics software package for education and data analysis. Palaeontol. Electron. 4, 1–9.

Heaton, T.J., Köhler, P., Butzin, M., Bard, E., Reimer, R.W., Austin, W.E.N., Bronk Ramsey, C., Grootes, P.M., Hughen, K.A., Kromer, B., Reimer, P.J., Adkins, J.F., Burke, A., Cook, M.S., Olsen, J., Skinner, L.C., 2020. Marine20—the marine radiocarbon age calibration curve (0–55,000 cal BP). Radiocarbon 62, 779–820. https://doi.org/10.1017/RDC.2020.68.

Hennekam, R., Donders, T.H., Zwiep, K., de Lange, G.J., 2015. Integral view of Holocene precipitation and vegetation changes in the Nile catchment area as inferred from its delta sediments. Quat. Sci. Rev. 130, 189–199. https://doi.org/10.1016/j.quascirev.2015.05.031.

Huntley, B., Birks, H.J.B., 1983. An atlas of past and present pollen maps for Europe: 0–13,000 years ago. Cambridge University Press, Cambridge.

Jorissen, F.J., 1988. Benthic Foraminifera From the Adriatic Sea: Principles of Phenotypic Variation. PhD Thesis. Utrecht University, Utrecht.

Jorissen, F., Nardelli, M.P., Almogi-Labin, A., Barras, C., Bergamin, L., Bicchi, E., El Kateb, A., Ferraro, L., McGann, M., Morigi, C., Romano, E., Spezzaferri, S., 2018. Developing Foram-AMBI for biomonitoring in the Mediterranean: species assignments to ecological categories. Mar. Micropaleontol. 140, 33–45. https://doi.org/10.1016/j.marmicro.2017.12.006.

Kaniewski, D., Marriner, N., Vacchi, M., Camuffo, D., Bivolaru, A., Sarti, G., Bertoni, D., Diatta, L., Markakis, N., Martella, A., Otto, T., Luce, F., Calaon, D., Cottica, D., Morhange, C., 2024. Holocene Sea-level impacts on Venice Lagoon's coastal wetlands. Glob. Planet. Chang. 236, 104426. https://doi.org/10.1016/j.gloplacha.2024.104426.

Kaniewski, D., van Campo, E., Paulissen, E., Weiss, H., Bakker, J., Rossignol, I., van Lerberghe, K., 2011. The medieval climate anomaly and the Little Ice Age in coastal Syria inferred from pollen-derived palaeoclimatic patterns. Global Planet. Change 78, 178–187. https://doi.org/10.1016/j.gloplacha.2011.06.010.

Kaplan, J.O., Krumhardt, K.M., Zimmermann, N., 2009. The prehistoric and preindustrial deforestation of Europe. Quat. Sci. Rev. 28, 3016–3034. https://doi.org/10.1016/j.quascirev.2009.09.028.

Köppen, W., 1936. Das geographische System der Klimatologie. Gebrüder Borntraeger, Berlin.

Kottek, M., Grieser, J., Beck, C., Rudolf, B., Rubel, F., 2006. World map of the Köppen–Geiger climate classification updated. Meteorol. Z. 15, 259–263. https://doi.org/10.1127/0941-2948/2006/0130.

Lambeck, K., Antonioli, F., Anzidei, M., Ferranti, L., Leoni, G., Scicchitano, G., Silenzi, S., 2011. Sea level change along the Italian coast during the Holocene and projections for the future. Quat. Int. 232, 250–257. https://doi.org/10.1016/j.quaint.2010.04.026.

Last, W.M., Smol, J.P. (Eds.), 2006. *Tracking Environmental Change Using Lake Sediments. Volume 1: Basin Analysis, Coring, and Chronological Techniques*. Developments in Paleoenvironmental Research 1. Springer, Dordrecht.

Lowe, J.J., Accorsi, C.A., Bandini Mazzanti, M., Bishop, V., van der Kaars, S., Forlani, L., Mercuri, A.M., Rivalenti, C., Torri, P., Watson, C., 1996. Pollen stratigraphy of sediment sequences from crater lakes Albano and Nemi (near Rome) and from the central Adriatic, spanning the interval from oxygen isotope stage 2 to the present day. Memorie dell'Istituto Italiano di Idrobiologia 55, 71–98.

Luterbacher, J., Rickli, R., Xoplaki, E., Tinguely, C., Beck, C., Pfister, C., Wanner, H., 2001. The late Maunder Minimum (1675–1715): a key period for studying decadal scale climatic change in Europe. Clim. Chang. 49, 441–462. https://doi.org/10.1023/A:1010667524422.

Magny, M., Vannière, B., de Beaulieu, J.L., Bégeot, C., Heiri, O., Millet, L., Peyron, O., Walter-Simonnet, A.V., 2007. Early-Holocene climatic oscillations recorded by lake-level fluctuations in west-central Europe and in central Italy. Quat. Sci. Rev. 26, 1951–1964.

Magny, M., Arnaud, F., Holzhauser, H., Chapron, E., Debret, M., Desmet, M., Leroux, A., Millet, L., Revel, M., Vannière, B., 2010. Solar and proxy-sensitivity imprints on paleohydrological records for the last millennium in west-central Europe. Quat. Res. 73, 173–179. https://doi.org/10.1016/j.yqres.2009.11.006.

Magny, M., Combourieu-Nebout, N., de Beaulieu, J.L., Bout-Roumazeilles, V., Colombaroli, D., Desprat, S., Francke, A., Joannin, S., Ortu, E., Peyron, O., Revel, M., Sadori, L., Siani, G., Sicre, M.A., Samartin, S., Simonneau, A., Tinner, W., Vannière, B., Wagner, B., Zanchetta, G., Anselmetti, F., Brugiapaglia, E., Chapron, E., Debret, M., Desmet, M., Didier, J., Essallami, L., Galop, D., Gilli, A., Haas, J.N., Kallel, N., Millet, L., Stock, A., Turon, J.L., Wirth, S., 2013. North–south palaeohydrological contrasts in the central Mediterranean during the Holocene: tentative synthesis and working hypotheses. Clim. Past 9, 2043–2071. https://doi.org/10.5194/cp-9-2043-2013.

Magri, D., Sadori, L., 1999. Late Pleistocene and Holocene pollen stratigraphy at Lago di Vico, central Italy. Veg. Hist. Archaeobotany 8, 247–260. https://doi.org/10.1007/BF01291777.

Magri, D., Agrillo, E., Di Rita, F., Furlanetto, G., Pini, R., Ravazzi, C., Spada, F., 2015. Holocene dynamics of tree taxa populations in Italy. Rev. Palaeobot. Palynol. 218, 267–284. https://doi.org/10.1016/j.revpalbo.2014.08.012.

Marchesini, M., Marvelli, S., 2017. Paesaggio vegetale e agricoltura nella Pianura Padana in età romana. In: Lo Cascio, E., Maiuro, M. (Eds.), Popolazione e Risorse nell'Italia del nord dalla Romanizzazione ai Longobardi, 28. Pragmateiai, Bari, pp. 289–304.

Marchesini, M., Marvelli, S., 2018. Paesaggio e ambiente in età romana nella bassa Pianura Padana. In: Cesarano, M., Vallicelli, V.C., Zamboni, L. (Eds.), Antichi Romani e Romanità nelle Terre del Delta del Po. Nuovi Studi e Prospettive di Ricerca, 8. Ricerche Series Maior, Bologna, pp. 115–125.

Maselli, V., Trincardi, F., 2013. Man made deltas. Sci. Rep. 3, 1926. https://doi.org/10.1038/srep01926.

Mayewski, P.A., Rohling, E.E., Stager, J.C., Karlén, W., Maasch, K.A., Meeker, L.D., Meyerson, E.A., Gasse, F., van Kreveld, S., Holmgren, K., Lee-Thorp, J., Rosqvist, G., Rack, F., Staubwasser, M., Schneider, R.R., Steig, E.J., 2004. Holocene climate variability. Quat. Res. 62, 243–255. https://doi.org/10.1016/j.yqres.2004.07.001.

Mercuri, A.M., Sadori, L., 2014. Mediterranean culture and climatic change: past patterns and future trends. In: Goffredo, S., Dubinsky, Z. (Eds.), The Mediterranean Sea: Its History and Present Challenges. Elsevier, Amsterdam, pp. 507–527.

Mercuri, A.M., Accorsi, C.A., Bandini Mazzanti, M., 2002. The long history of *Cannabis* and its cultivation by the Romans in central Italy, shown by pollen records from Lago Albano and Lago di Nemi. Veg. Hist. Archaeobotany 11, 263–276. https://doi.org/10.1007/s003340200039.

Mercuri, A.M., Mazzanti, M.B., Torri, P., Vigliotti, L., Bosi, G., Florenzano, A., Olmi, L., N'siala, I.M., 2012. A marine/terrestrial integration for mid-late Holocene vegetation history and the development of the cultural landscape in the Po valley as a result of human impact and climate change. Veg. Hist. Archaeobotany 21, 353–372. https://doi.org/10.1007/s00334-012-0352-4.

Mercuri, A.M., Bandini Mazzanti, M., Florenzano, A., Montecchi, M.C., Rattighieri, E., 2013. *Olea*, *Juglans* and *Castanea*: the OJC group as pollen evidence of the development of human-induced environments in the Italian peninsula. Quat. Int. 303, 24–42. https://doi.org/10.1016/j.quaint.2013.01.005.

Milker, Y., Schmiedl, G., 2012. A taxonomic guide to modern benthic shelf foraminifera of the western Mediterranean Sea. Palaeontol. Electron. 15, 1–134. https://doi.org/10.26879/271.

Milli, S., D'Ambrogi, C., Bellotti, P., Calderoni, G., Carboni, M.G., Celant, A., Di Bella, L., Di Rita, F., Frezzotti, M., Magri, D., Ricci, V., 2013. The transition from wave-dominated estuary to wave-dominated delta: the Late Quaternary stratigraphic architecture of Tiber River deltaic succession (Italy). Sediment. Geo. 284, 159–180. https://doi.org/10.1016/j.sedgeo.2012.12.003.

Moore, P.D., Webb, J.A., Collinson, M.E., 1991. Pollen Analysis, 2nd ed. Blackwell Scientific Publications, Oxford.

Mudie, P.J., McCarthy, F.M., 2006. Marine palynology: potentials for onshore–offshore correlation of Pleistocene–Holocene records. Trans. R. Soc. S. Afr. 61, 139–157. https://doi.org/10.1080/00359190609519957.

Nelson, B.W., 1970. Hydrography, sediment dispersal, and recent historical development of the Po River delta, Italy. In: Morgan, J.P., Shaver, R.H. (Eds.), Deltaic Sedimentation: Modern and Ancient, 15. SEPM (Society of Economic Paleontologists and Mineralogists) Special Publication, Tulsa, pp. 152–184. https://doi.org/10.2110/pec.70.11.0152.

Nummedal, D., Swift, D.J.P., 1987. Transgressive stratigraphy at sequence-bounding unconformities: some principles derived from Holocene and Cretaceous examples. In: Nummedal, D., Pilkey, O.H., Howard, J.D. (Eds.), Sea-Level Fluctuation and Coastal Evolution, 41. SEPM (Society of Economic Paleontologists and Mineralogists) Special Publication, Tulsa, pp. 241–260. https://doi.org/10.2110/pec.87.41.0241.

Oldfield, F., Asioli, A., Accorsi, C.A., Mercuri, A.M., Juggins, S., Langone, L., Rolph, T., Trincardi, F., Wolff, G., Gibbs, Z., Vigliotti, L., Frignani, M., van der Post, K., Branch, N., 2003. A high resolution late Holocene palaeo environmental record from the central Adriatic Sea. Quat. Sci. Rev. 22, 319–342. https://doi.org/10.1016/S0277-3791(02)00088-4.

Orlić, M., Gačić, M., La Violette, P.E., 1992. The currents and circulation of the Adriatic Sea. Oceanol. Acta 15, 109–124.

Orlić, M., Kuzmić, M., Pasarić, Z., 1994. Response of the Adriatic Sea to the bora and sirocco forcing. Continental Shelf Res. 14, 91–116. https://doi.org/10.1016/0278-4343(94)90007-8.

Ostrogorski, G., 1968. Storia dell'Impero bizantino. Einaudi, Torino.

Palli, J., Fiolna, S., Bini, M., Cappella, F., Izdebski, A., Masi, A., Regattieri, E., Zanchetta, G., 2025. The human-driven ecological success of olive trees over the last 3700 years in the Central Mediterranean. Quat. Sci. Rev. 356, 109313. https://doi.org/10.1016/j.quascirev.2025.109313.

Peel, M.C., Finlayson, B.L., McMahon, T.A., 2007. Updated world map of the Köppen-Geiger climate classification. Hydrol. Earth Syst. Sci. 11, 1633–1644. https://doi.org/10.5194/hess-11-1633-2007.

Pellegrini, C., Maselli, V., Cattaneo, A., Piva, A., Ceregato, A., Trincardi, F., 2015. Anatomy of a compound delta from the post-glacial transgressive record in the Adriatic Sea. Mar. Geol. 362, 43–59.
Pellegrini, C., Sammartino, I., Schieber, J., Tesi, T., Paladini de Mendoza, F., Rossi, V., Amorosi, A., 2024. On depositional processes governing along-strike facies variations of fine-grained deposits: unlocking the Little Ice Age subaqueous clinothems on the Adriatic shelf. Sedimentology 71, 941–973. https://doi.org/10.1111/sed.13162.
Pellegrini, C., Tesi, T., Schieber, J., Bohacs, K.M., Rovere, M., Asioli, A., Correggiari, A., Cattaneo, A., Trincardi, F., 2021. Fate of terrigenous organic carbon in muddy clinothems on continental shelves revealed by stratal geometries: insight from the Adriatic sedimentary archive. Global Planet. Change 203, 103539. https://doi.org/10.1016/j.gloplacha.2021.103539.
Pennington, B.T., Sturt, F., Wilson, P., Rowland, J., Brown, A.G., 2017. The fluvial evolution of the Holocene Nile Delta. Quat. Sci. Rev. 170, 212–231. https://doi.org/10.1016/j.quascirev.2017.06.017.
Piccoli, F., Gerdol, R., Ferrari, C., 1983. Carta della vegetazione del Bosco della Mesola (Ferrara), 2. Atti dell'Istituto di Botanica e del Laboratorio Crittogamico dell'Università di Pavia, pp. 1–32.
Pignatti, S., 1979. I piani di vegetazione in Italia. Plant Biosyst. 113, 411–428.
Pignatti, S., Guarino, R., La Rosa, M., 2017–2019. Flora d'Italia. Edagricole, Bologna.
Punt, W., Bos, J.A., Hoen, P.P., 1991. Oleaceae. Rev. Palaeobot. Palynol. 69, 23–47.
Punt, W., Malotaux, M., 2007. Cannabaceae, moraceae and urticaceae. Rev. Palaeobot. Palynol. 146, 23–44.
Punt, W., van Benthem, F., Clarke, G.C.S., 1984. Fagaceae. Rev. Palaeobot. Palynol. 42, 87–110.
Rasmussen, T.L., Thomsen, E., Skirbekk, K., Ślubowska-Woldengen, M., Klitgaard Kristensen, D., Koç, N., 2014. Spatial and temporal distribution of Holocene temperature maxima in the northern Nordic seas: interplay of Atlantic-, Arctic- and polar water masses. Quat. Sci. Rev. 92, 280–291. https://doi.org/10.1016/j.quascirev.2013.10.034.
Regattieri, E., Zanchetta, G., Isola, I., Zanella, E., Drysdale, R.N., Hellstrom, J.C., Galli, E., Magrì, F., 2019. Holocene Critical Zone dynamics in an Alpine catchment inferred from a speleothem multiproxy record: disentangling climate and human influences. Sci. Rep. 9, 17829. https://doi.org/10.1038/s41598-019-53,583-7.
Reille, M., 1992. Pollen et spores d'Europe et d'Afrique du Nord. Laboratoire de Botanique Historique et Palynologie, Marseille.
Reille, M., 1995. Pollen et spores d'Europe et d'Afrique du Nord. Supplément 1. Laboratoire de Botanique Historique et Palynologie, Marseille.
Reille, M., 1998. Pollen et spores d'Europe et d'Afrique du Nord. *Supplément 2.* Laboratoire de Botanique Historique et Palynologie, Marseille.
Reimer, P.J., Austin, W.E.N., Bard, E., Bayliss, A., Blackwell, P.G., Bronk Ramsey, C., Butzin, M., Cheng, H., Edwards, R.L., Friedrich, M., Grootes, P.M., Guilderson, T.P., Hajdas, I., Heaton, T.J., Hogg, A.G., Hughen, K.A., Kromer, B., Manning, S.W., Muscheler, R., Palmer, J.G., Pearson, C., van der Plicht, J., Reimer, R.W., Richards, D.A., Scott, E.M., Southon, J.R., Turney, C.S.M., Wacker, L., Adolphi, F., Büntgen, U., Capano, M., Fahrni, S.M., Fogtmann-Schulz, A., Friedrich, R., Köhler, P., Kudsk, S., Miyake, F., Olsen, J., Reinig, F., Sakamoto, M., Sookdeo, A., Talamo, S., 2020. The IntCal20 Northern Hemisphere radiocarbon age calibration curve (0–55 cal kBP). Radiocarbon 62, 725–757. https://doi.org/10.1017/RDC.2020.41.
Renaud, F.G., Syvitski, J.P., Sebesvari, Z., Werners, S.E., Kremer, H., Kuenzer, C., Friedrich, J., 2013. Tipping from the Holocene to the Anthropocene: how threatened are major world deltas? Curr. Opin. Environ. Sustain. 5, 644–654. https://doi.org/10.1016/j.cosust.2013.11.007.
Roberts, N., Brayshaw, D., Kuzucuoğlu, C., Perez, R., Sadori, L., 2011. The mid-Holocene climatic transition in the Mediterranean: causes and consequences. The Holocene 21, 3–13. https://doi.org/10.1177/0959683610388058.
Roberts, N., Fyfe, R.M., Woodbridge, J., Gaillard, M.-J., Davis, B.A.S., Kaplan, J.O., Marquer, L., Mazier, F., Nielsen, A.B., Sugita, S., Trondman, A.-K., Leydet, M., 2018. Europe's lost forests: a pollen-based synthesis for the last 11,000 years. Sci. Rep. 8, 716. https://doi.org/10.1038/s41598-017-18,646-7.
Rossi, V., Vaiani, S.C., 2008. Benthic foraminiferal evidence of sediment supply changes and fluvial drainage reorganization in Holocene deposits of the Po Delta, Italy. Mar. Micropaleontol. 69, 106–118.
Rossi, V., Barbieri, G., Vaiani, S.C., Cacciari, M., Bruno, L., Campo, B., Marchesini, M., Marvelli, S., Amorosi, A., 2021. Millennial-scale shifts in microtidal ecosystems during the Holocene: dynamics and drivers of change from the Po Plain coastal record (NE Italy). J. Quat. Sci. 36, 961–979. https://doi.org/10.1002/jqs.3322.
Ruddiman, W.F., 2003. The anthropogenic greenhouse era began thousands of years ago. Clim. Chang. 61, 261–293. https://doi.org/10.1023/B:CLIM.0000004577.17928.fa.
Sadori, L., Mercuri, A.M., Mariotti Lippi, M., 2010. Reconstructing past cultural landscape and human impact using pollen and plant macroremains. Plant Biosyst. 144, 940–951. https://doi.org/10.1080/11263504.2010.491982.
Sadori, L., Bertini, A., Combourieu-Nebout, N., Kouli, K., Mariotti Lippi, M., Roberts, N., Mercuri, A.M., 2013. Palynology and Mediterranean vegetation history. Flora Mediterr. 23, 141–156. https://doi.org/10.7320/FlMedit23.141.
Scarponi, D., Nawrot, R., Azzarone, M., Pellegrini, C., Gamberi, F., Trincardi, F., Kowalewski, M., 2022. Resilient biotic response to long-term climate change in the Adriatic Sea. Glob. Chang. Biol. 28, 4041–4053. https://doi.org/10.1111/gcb.16168.
Sgarrella, F., Moncharmont Zei, M., 1993. Benthic foraminifera of the Gulf of Naples (Italy): systematics and autoecology. Boll. Soc. Paleontol. Ital. 32, 145–264.
Simeoni, U., Corbau, C., 2009. A review of the Delta Po evolution (Italy) related to climatic changes and human impacts. Geomorphology 107, 64–71. https://doi.org/10.1016/j.geomorph.2008.11.004.
Soboyejo, L.A., Giambastiani, B.M.S., Molducci, M., Antonellini, M., 2021. Different processes affecting long-term Ravenna coastal drainage basins (Italy): implications for water management. Environ. Earth Sci. 80, 493. https://doi.org/10.1007/s12665-021-09774-5.
Soldati, M., Marchetti, M. (Eds.), 2017. Landscapes and landforms of Italy. Springer, Cham. https://doi.org/10.1007/978-3-319-26,194-2.
Stanley, D.J., Warne, A.G., 1994. Worldwide initiation of holocene marine deltas by deceleration of sea-level rise. Science 265, 228–231. https://doi.org/10.1126/science.265.5169.228.
Stefani, M., Vincenzi, S., 2005. The interplay of eustasy, climate and human activity in the late Quaternary depositional evolution and sedimentary architecture of the Po Delta system. Mar. Geol. 222–223, 19–48. https://doi.org/10.1016/j.margeo.2005.06.029.
Steinhilber, F., Beer, J., Fröhlich, C., 2009. Total solar irradiance during the Holocene. Geophys. Res. Lett. 36, L19704. https://doi.org/10.1029/2009GL040142.
Swarzenski, P.W., 2014. 210Pb dating. In: Rink, W.J., Thompson, J.W. (Eds.), Encyclopedia of Scientific Dating Methods. Springer, Dordrecht, pp. 1–11. https://doi.org/10.1007/978-94-007-6326-5_236–1.
Syvitski, J.P.M., Kettner, A.J., 2007. On the flux of water and sediment into the Northern Adriatic Sea. Cont. Shelf Res. 27, 296–308. https://doi.org/10.1016/j.csr.2005.08.029.
Syvitski, J.P., Kettner, A.J., Overeem, I., Hutton, E.W., Hannon, M.T., Brakenridge, G.R., Day, J., Vörösmarty, C., Saito, Y., Giosan, L., Nicholls, R.J., 2009. Sinking deltas due to human activities. Nat. Geosci. 2, 681–686. https://doi.org/10.1038/ngeo629.
Tarasov, P.E., Cheddadi, R., Guiot, J., Bottema, S., Peyron, O., Belmonte, J., Ruiz-Sanchez, V., Saadi, F., Brewer, S., 1998. A method to determine warm and cool steppe biomes from pollen data; application to the Mediterranean and Kazakhstan regions. J. Quat. Sci. 13 (4), 335–344. https://doi.org/10.1002/(SICI)1099-1417(199807/08)13:43.3.CO;2-1.
Tomaselli, M., 1970. Note Illustrative Alla Carta Della Vegetazione Naturale Potenziale.
Trincardi, F., Amorosi, A., Bosman, A., Correggiari, A., Madricardo, F., Pellegrini, C., 2020. Ephemeral rollover points and clinothem evolution in the modern Po Delta based on repeated bathymetric surveys. Basin Res. 32, 402–418. https://doi.org/10.1111/bre.12426.
Tüxen, R., 1956. Die heutige potentielle natürliche Vegetation als Gegenstand der Vegetationskartierung. Angew. Pflanzensoziologie 13, 5–42.
Vacchi, M., Marriner, N., Morhange, C., Spada, G., Fontana, A., Rovere, A., 2016. Multiproxy assessment of Holocene relative sea-level changes in the western Mediterranean: sea-level variability and improvements in the definition of the isostatic signal. Earth Sci. Rev. 155, 172–197. https://doi.org/10.1016/j.earscirev.2016.02.002.
Van De Schootbrugge, B., Koutsodendris, A., Taylor, W., Weston, F., Wellman, C., Strother, P.K., 2024. Recognition of an extended record of euglenoid cysts: implications for the end-Triassic mass extinction. Rev. Palaeobot. Palynol. 322, 105043. https://doi.org/10.1016/j.revpalbo.2023.105043.
Veggiani, A., 1990. Fluttuazioni climatiche e trasformazioni ambientali nel territorio imolese dall'alto medioevo all'età moderna. In: Mancini, F., Gioberti, M., Veggiani, A. (Eds.), Imola nel Medioevo, pp. 41–102. Imola.
Vona, I., Colella, S., Sammartino, M., Brando, V.E., Falcini, F., 2025. Positive correlation between the Po River discharge and ocean colour trends of Chl and TSM in the Adriatic Sea. Front. Remote Sens. 6, 1574347. https://doi.org/10.3389/frsen.2025.1574347.
Walker, M.J.C., Berkelhammer, M., Björck, S., Cwynar, L.C., Fisher, D.A., Long, A.J., Lowe, J.J., Newnham, R.M., Rasmussen, S.O., Weiss, H., 2012. Formal subdivision of the Holocene Series/Epoch: a discussion paper by a working group of INTIMATE (Integration of ice-core, marine and terrestrial records) and the Subcommission on Quaternary Stratigraphy (International Commission on Stratigraphy). J. Quat. Sci. 27, 649–659. https://doi.org/10.1002/jqs.2565.
Wanner, H., Solomina, O., Grosjean, M., Ritz, S.P., Jetel, M., 2011. Structure and origin of Holocene cold events. Quat. Sci. Rev. 30, 3109–3123. https://doi.org/10.1016/j.quascirev.2011.07.010.
Wanner, H., Pfister, C., Neukom, R., 2022. The variable European little ice age. Quat. Sci. Rev. 287, 107531. https://doi.org/10.1016/j.quascirev.2022.107531.
Zamboni, L., 2021. The urbanization of northern Italy: contextualizing early settlement nucleation in the Po Valley. J. Archaeol. Res. 29, 387–430.
Zhao, X., Kaniewski, D., Wang, Y., Marriner, N., Salem, A., Alassal, S.E., Liu, Y., Jiang, F., Chen, J., Sun, Q., Li, M., Thomas, I., Finlayson, B., Sheisha, H., Morhange, C., Otto, T., Luce, F., Chen, Z., 2025. On the long and winding road: unravelling the late emergence of Neolithic agriculture in the Nile Delta. Quat. Sci. Rev. 359, 109368. https://doi.org/10.1016/j.quascirev.2025.109368.
Zonneveld, K.A.F., Harper, K., Klügel, A., Chen, L., De Lange, G.J., Versteegh, G.J.M., 2024. Climate change, society, and pandemic disease in Roman Italy between 200 BCE and 600 CE. Sci. Adv. 10, eadk1033. https://doi.org/10.1126/sciadv.adk1033.